Broadband configurations for the Square Kilometer Array

Mugni, N.M.C.

Award date:
2000

FACULTEIT ELEKTROTECHNIEK

CAPACITEITSGROEP TTE

LEERSTOELGEBIED Elektromagnetisme

Broadband Configurations for the Square Kilometer Array

door

N.M.C. Mugni

EM-3-00

Verslag van een afstudeeronderzoek,
verricht in de capaciteitsgroep TTE,
onder begeleiding van
Prof .Dr. A.G. Tijhuis,
Dr. Ir. A.B. Smolders en
Dr. C. Craye
in de periode van september 1999 - juni 2000.

Eindhoven, juni 2000.

Contents

Chapter 1

Introduction

The need for a new generation of radio telescopes arose in the 1990's when astronomers expressed the desire to observe the first galaxies which were created just after the Big Bang. To achieve this purpose, this new telescope should be a hundred times more sensitive to radio signals from the sky than telescopes in use and it should operate over a frequency decade, from 200 MHz to 2 GHz. An international radio astronomy committee [1], [2] defined more characteristics and a scientific program led by the Netherlands Foundation for Research in Astronomy (NFRA), was started in 1995.

A sub-microjansky sensitivity is required to observe the birth of the Universe and can be reached in different ways. A team of Chinese researchers involved in the program tries to find a solution with parabolic dishes whereas the NFRA examines an option based on the concept of a phased array antenna. In that case, the specified sensitivity imposes a collecting area of roughly one square kilometer from which comes the name of the telescope: the Square Kilometer Array (SKA).

Besides the unprecedented sensitivity the necessity of coverage the whole of the sky imposes a configuration of 32 interferometer stations. These stations will each have a diameter of about 300 meters and will cover a region of 300×300 km as shown in Figure 1. Each station will be a phased array antenna composed of more than a million elements connected by a beamforming network.

Celestial signals from distant radio sources are weak and flooded with noise due to human activities, such as wireless communication and TV transmissions. With a phased array, these interferences can be conveniently suppressed by using a technique called adaptive spatial nulling. In addition, a phased array enables easy tracking of sources due to an electronical beamforming and offers the possibility for several observations simultaneously.

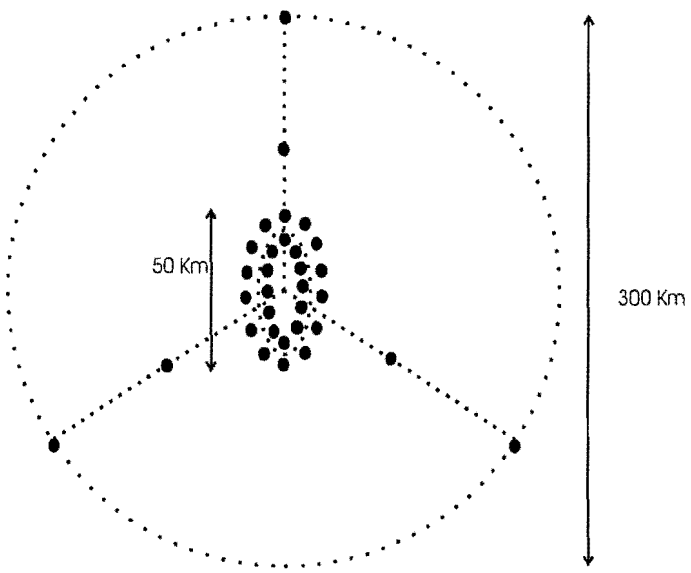

Figure 1. The collecting area of SKA is distributed over 32 stations. The central region provides sensitivity and the outlying stations resolution.

For a uniformly spaced array, grating lobes appear as soon as the inter-element spacing is more than half of a wavelength. SKA should have a broadband behaviour over a decade from 200 MHz to 2 GHz. Thus, inter-element spacing should be 7.5 cm in order to avoid grating lobes at the highest frequency. This leads to a requirement of roughly 12 million elements per station. In terms of cost, this condition is unacceptable. Therefore, different techniques have been studied to suppress the grating lobes while keeping a low number of elements. It turns out that the array should be configured with unequally spaced elements.

In this report, a theoretical development is conducted to understand the problem. Then, three types of design approaches are identified after an exhaustive literature review. These procedures are studied in depth. Finally, a full comparison between these configurations is done. A software package, based on the theory described in this report, is available.

Chapter 2

Array fundamentals

In this chapter, we present some theoretical elements in the description of an array. We shall begin the discussion with the simplest configuration possible: an array of isotropic radiators (radiating elements) equally spaced along a line (linear in a geometric sense). It will be seen that the more complex array theory can be framed as an extension of this simple case. Finally, we will show why SKA should not be constructed as a regular array.

2.1 The linear phased array

2.1.1 Array factor

Let us consider the elementary array shown in Figure 2.1. It consists of N isotropic radiators with a constant spacing d. On reception, a plane wave is incident upon the array from a direction making an angle θ with respect to the array normal. The current in the n^{th} element will be of the form

$$i_n' = Ae^{jnkd\sin\theta}, \qquad (2.1)$$

where A is a complex constant related to the instantaneous amplitude and phase of the plane wave and k is the wavenumber

$$k = \frac{2\pi f}{c} = \frac{2\pi}{\lambda}, \qquad (2.2)$$

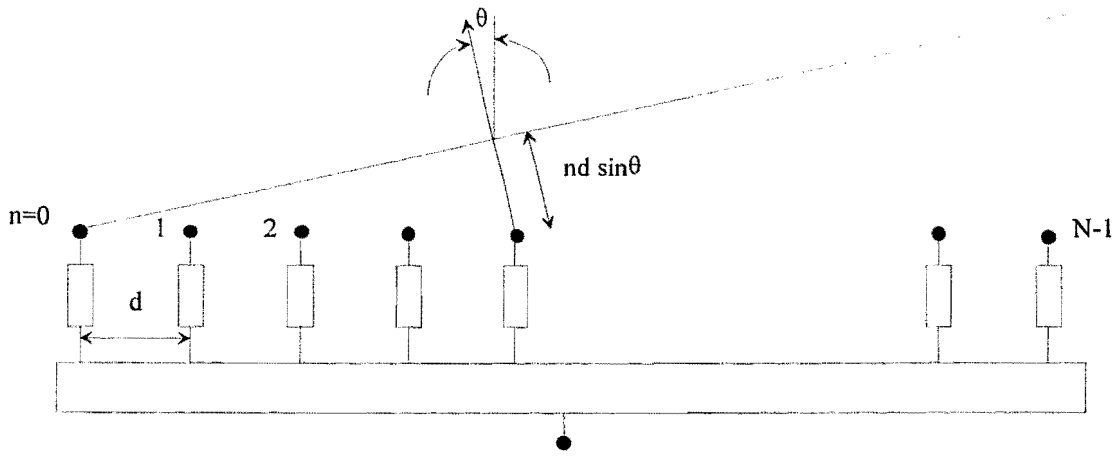

Fig.2.1. The basic linear-array configuration.

where f is the frequency and c is the velocity of light in vacuum. From Equation (2.1) it can be seen that the phase of the current in the n^{th} element leads that of the $(n+1)^{th}$ element by a phase shift given by $\Delta\varphi = kd \sin\theta$. This phase shift corresponds to a difference of $\tau = d/c \sin\theta$ in the time of arrival of the plane wavefront. If we place a control element behind each receiver, as indicated in Figure 2.1, the transfer coefficient for the n^{th} element is given by

$$\frac{i''}{i'} = a_n e^{j\varphi_n}, \qquad (2.3)$$

where a_n and φ_n are the real current gain and phase shift respectively for each element. Then, combining (2.1) and (2.3), the addition network produces an output current

$$I(\theta) = \sum_{n=0}^{N-1} a_n e^{j(\varphi_n + nkd\sin\theta)}. \qquad (2.4)$$

This relationship gives the response of the array shown in Figure 2.1. The set of coefficients $\{a_n\}$ is usually called the *array amplitude taper*, while the set of a phase shifts $\{\varphi_n\}$ is called the *phase taper*. The sum in equation (2.2) is called the ***array factor***. The signals received from all the radiators must be combined in phase. Therefore to obtain a maximum response in the scan direction, θ_0, the phase φ_n must have the form

$$\varphi_n = -nkd\sin\theta_0 \ . \qquad (2.5)$$

This expression shows that a linear phase is required across the array aperture to achieve a constant phase difference between adjacent radiators. Substituting (2.5) into (2.4) yields the array factor,

$$E_a(\theta) = \sum_{n=0}^{N-1} a_n e^{jnkd(\sin\theta - \sin\theta_0)} \qquad (2.6)$$

In the special case of a uniformly illuminated array ($a_n = 1$ for all n), the array factor of an N-element array becomes

$$|E_a(\theta)| = \left| \frac{\sin[N\frac{kd}{2}(\sin\theta - \sin\theta_0)]}{N\sin[\frac{kd}{2}(\sin\theta - \sin\theta_0)]} \right| \qquad (2.7)$$

2.1.2 Visible region and grating lobes

- *Visible region*

It is convenient to express the array factor in terms of the variable, $u = \sin\theta$, as follows,

$$E_a(u) = \sum_{n=0}^{N-1} a_n e^{jnkd(u-u_0)} \qquad (2.8)$$

the scanning direction $u_0 = \sin\theta_0$ is related to the differential phase shift by $\varphi_0 = -kd\,u_0$. $E_a(u)$ and $E_a(\theta)$ are related by a one-to-one mapping in the region $|u| \leq 1$. This is often referred to as the ***visible region***, corresponding to a real angle θ,

$$-\frac{\pi}{2} \leq \theta \leq \frac{\pi}{2},$$

or

$$-kd \leq kd.\sin\theta \leq kd \ . \qquad (2.9)$$

Hence, on the u-axis the visible region is limited to a segment of length $2kd$, centred about u_0 for a beam steered in a direction u_0. Equation (2.9) shows that the visible region depends on both the inter-element spacing, and the frequency. We can express the spacing in terms of a fraction of the wavelength, to obtain a dependence in terms of one variable only

$$kd = \frac{2\pi}{\lambda} x\lambda = 2\pi x$$

In the following discussion, we express all the distances in fraction of wavelength.

- *Grating lobes*

The array factor $E_a(u)$, is a periodic function of u with period,

$$\frac{2\pi}{kd} = \frac{1}{d/\lambda} = \frac{\lambda}{d}$$

and its expression in Equation (2.6) is in the form of a Fourier-series representation, which is readily analyzable and easy to visualize. With a uniform amplitude, $a_n=1$, the maxima of $E_a(u)$ occur when $kd(u-u_0) = 2p\pi$, where p is an integer

$$u_p - u_0 = \frac{p\lambda}{d} \qquad (2.10)$$

The maximum where $u_p = u_0$ or $p = 0$, is generally referred to as the *principal lobe or* ***main lobe***, and the other maxima are known as the ***grating lobes***. Figure 2.2 illustrates Equation (2.6); the grating lobes and the visible region location are indicated.

In the design of phased arrays, it is imperative to eliminate the grating lobes within the visible region since they lobes reduce the power in the main beam and thus reduce the antenna gain. The grating lobes can be eliminated by a proper choice of dimensions or by a proper design of the antenna element or both. They also may be avoided by non-uniform spacing of the antenna elements. We will examine this proposition in Chapter 3.

The condition to avoid grating lobes is that the spacing between lobes (λ/d) should be equal to or larger than the scan sector. For example, in an array steered to broadside, the first grating lobes appear on the horizon when $d = \lambda$. Thus a value of d slightly smaller than one wavelength ensures no large, spurious response to signals arriving from another direction. To avoid grating lobes at extreme steering angles, $u=\pm 1$, the lobe separation (in units of $u = \sin\theta$) should be two or larger. Hence the condition for avoidance of all grating lobes under all conditions of beam-steering is

$$d \le \frac{\lambda}{2} \qquad (2.11)$$

Equation (2.11) is closely related to the Nyquist sampling theorem in communication theory. We will go elaborate on that in section 2.2.2.

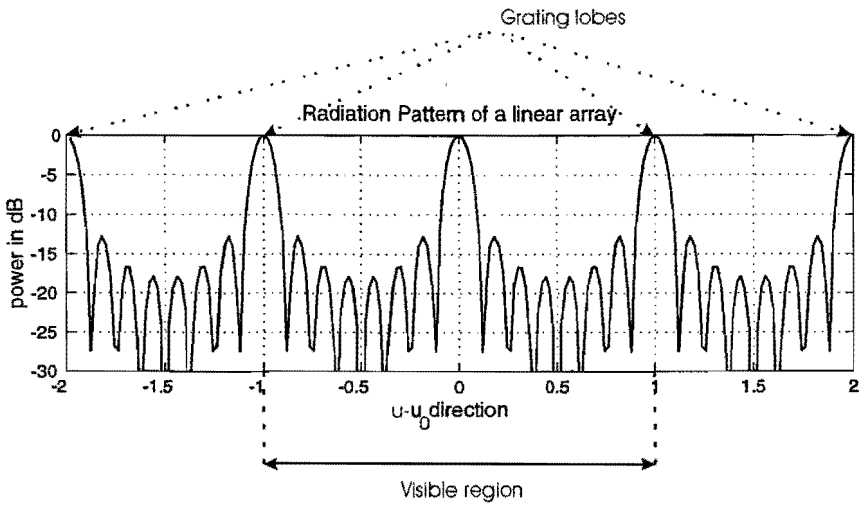

Figure 2.2. Radiation pattern of a 8-element linear array with an inter-element spacing $d=\lambda$

In summary, the inter-element spacing, expressed in terms of wavelength, determines the visible region of the array factor. Grating lobes enter the visible region as soon as the spacing is larger than $\lambda/2$. In Chapter 3, we will see that this rule does not apply to an array with unequally spaced elements. To be clear on the terminology, an unequally spaced element array, or a non-uniformly spaced element array, or an aperiodic array, or a non-regular array, refer to the same kind of array.

2.2 The planar phased array

2.2.1 Array factor, visible region and grating lobes

The results established in Section 2.1 for the linear phased array can be readily extended to the two dimensional array. A planar array of $N\times M$ isotropic radiators elements is depicted in Figure 2.3. In a rectangular lattice, the mn^{th} element is located at $x_m=md_x$ and $y_n=nd_y$. In a spherical coordinate system, the beam direction is defined by the two coordinates θ and ϕ. Thus, the array factor of a two-dimensional array is calculated by summing the vector contribution of each element in the array at each point in space. Then, the array factor can be written in terms of u and v as follows:

$$E_a(u,v)=\sum_m \sum_n i_{mn} e^{jk(md_x u+nd_y v)} \qquad (2.12)$$

$$\text{where} \quad \begin{aligned} u &= \sin\theta\cos\phi \\ v &= \sin\theta\sin\phi \end{aligned}$$

For a uniformly illuminated ($i_{mn}=1$) rectangular array, we can evaluate each sum of Equation (2.11), yielding,

$$\left|E_a(u,v)\right| = \frac{\left|\sin\left(\pi M\frac{d_x}{\lambda}u\right)\right|}{\left|M\sin\left(\pi\frac{d_x}{\lambda}u\right)\right|}\cdot\frac{\left|\sin\left(\pi N\frac{d_y}{\lambda}v\right)\right|}{\left|N\sin\left(\pi\frac{d_y}{\lambda}v\right)\right|} \qquad (2.13)$$

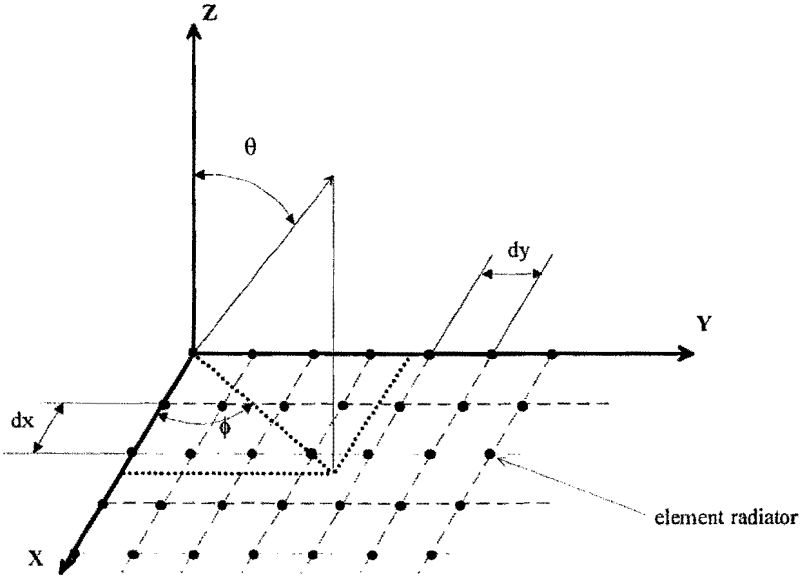

Figure 2.3. Element geometry of two-dimensional array.

As with a linear array, beam scanning is accomplished by linear phasing along both array coordinates. To scan the beam to the angular position corresponding to the directions defined by (u_0 ,v_0) a linear shift is introduced so that the excitation at the mn^{th} element is given by

$$i_{mn} = a_{mn}e^{jk(md_xu_0+nd_yv_0)}$$

Where kd_xu_0 is the element-to-element phase shift in the x-direction, and kd_yv_0 is the element-to-element phase shift in the y-direction. This form of phase steering indicates that the phase of the mn^{th} element is the sum of a row phase mkd_xu_0 and a

column phase $nkd_y v_0$. The array factor of a rectangular planar array of $M \times N$ elements is then given by

$$E_a(u,v) = \sum_m \sum_n a_{mn} e^{jk[md_x(u-u_0)+nd_y(v-v_0)]} \qquad (2.14)$$

The visible region is again defined by real angles of θ and ϕ. If we express this condition in terms of u and v, we end up with a visible region whose boundary is defined by the relation, $u^2+v^2=1$. So, the visible region of a planar array is a unit-circle in the (u,v) space. For a beam steered in a direction (u_o, v_0), the visible region is centred about (u_o, v_0) within a region whose boundary is $u^2+v^2=2$. Again, the visible region is frequency dependent, as we have seen in Section 2.1.2.

As it has been established for a linear array, the avoidance of grating lobes for all scan angles imposes an inter-element spacing of less than half a wavelength in both x and y-directions for a planar array. Figure 2.4 shows the radiation pattern for the configuration described in Figure 2.3. The computation has been carried out with an inter-element spacing of one wavelength along the two directions.

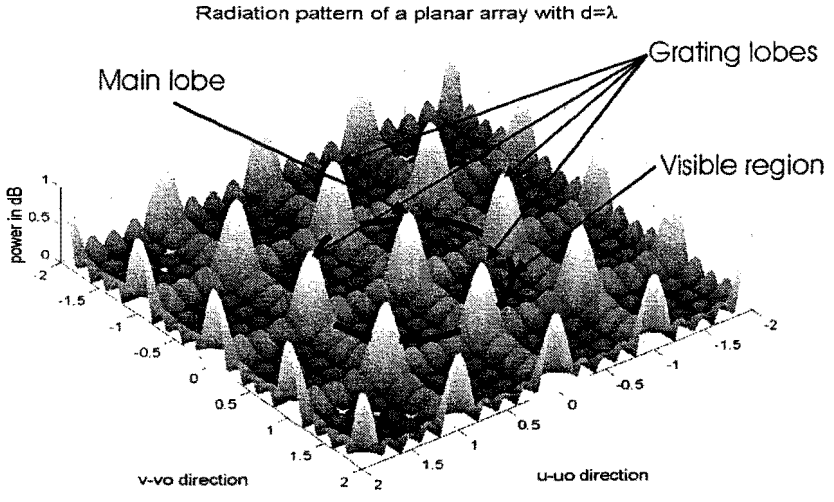

Figure 2.4. Radiation pattern of a planar array with $d=\lambda$

2.2.2 The Fourier approach

An array can be viewed as a sampled aperture antenna. If we consider a linear continuous aperture with a continuous current distribution $i_0(x)$, the corresponding array will be made of N elements exited by a current $i(x_n)$ placed at certain locations. These locations are determined by a sampling function. The sampling function is in general modelled with Dirac delta functions. As an example, let us consider a linear continuous antenna of length L with a constant current distribution, $i_0(x) = rectL$. If we sample this aperture with a sampling function s, chosen in such a way that $s(x)=\sum\delta(x-x_n)$, where $x_n=nd$ with d the sampling step ($L = nd$). The array current distribution $I(x)$ would result from the multiplication of the current distribution along the aperture by the sampling function,

$$\begin{aligned} I(x) &= i_0(x)s(x) \\ &= rect\ L \sum_{n=-\infty}^{\infty}\delta(x-nd) \end{aligned} \tag{2.15}$$

The far-field pattern of a linear or planar aperture is the Fourier transform of its current distribution. Thus, to obtain the far-field of the array current distribution $I(x)$, we take the Fourier transform of (2.15). We use also the following calculation rules used for a Fourier transformation: a multiplication gives a convolution in the Fourier space, the Fourier transform of an infinite series of delta function is also a series of delta function. It yields

$$\begin{aligned} E(u) &= FT\{rect\ L\} * FT\left\{\sum_{-\infty}^{\infty}\delta(x-nd)\right\} \\ &= \frac{\sin(\pi Lu/\lambda)}{\pi Lu/\lambda} * \sum_{-\infty}^{\infty}\delta(u-\frac{m\lambda}{d}) \end{aligned} \tag{2.16}$$

Figure 2.5 illustrates Equation (2.16). So, the radiation pattern is the convolution between the Fourier transform of the aperture current distribution and the Fourier transform of the sampling function. Notice that the inter-element spacing determines the position of the grating lobes: the smaller the inter-element spacing, the larger the distance between the grating lobes.

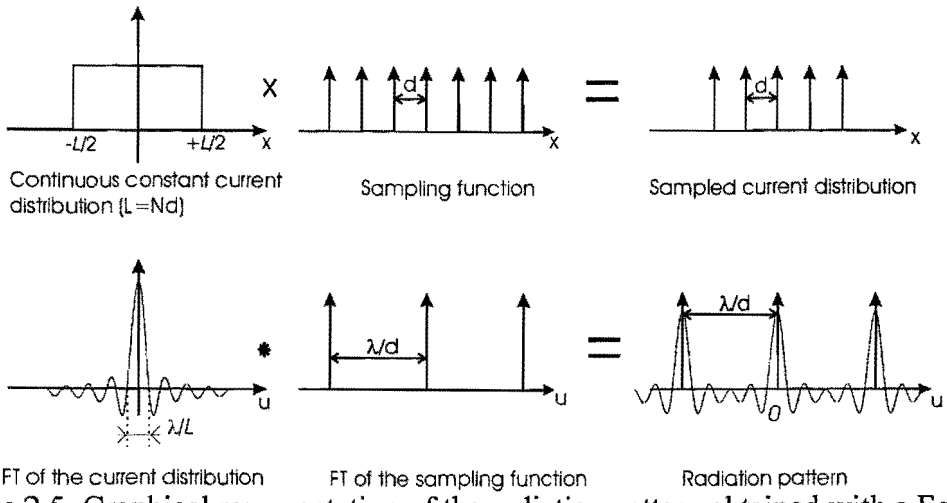

Figure 2.5. Graphical representation of the radiation pattern obtained with a Fourier approach.

The same procedure can be applied in two dimensions. As with the linear array, the radiation pattern of a planar array can be expressed as the convolution between the Fourier transform of a two-dimensional sampling function and the Fourier transform of the aperture antenna current distribution.

Many of the important properties of arrays can be determined by independently studying the sampled function and the current distribution over the aperture. Let us first focus on the current distribution. A well-known technique used to control the side lobes in the radiation pattern is the *amplitude taper* technique. It consists in applying a specified current distribution along the antenna aperture. From Fourier theory we know that an abrupt change in the current distribution will lead to high side-lobe level in the radiation pattern. Therefore, a smooth cosine current distribution results in lower side lobes than a rectangular distribution with a sharp discontinuity at the edge. This is shown graphically in Figure 2.6.

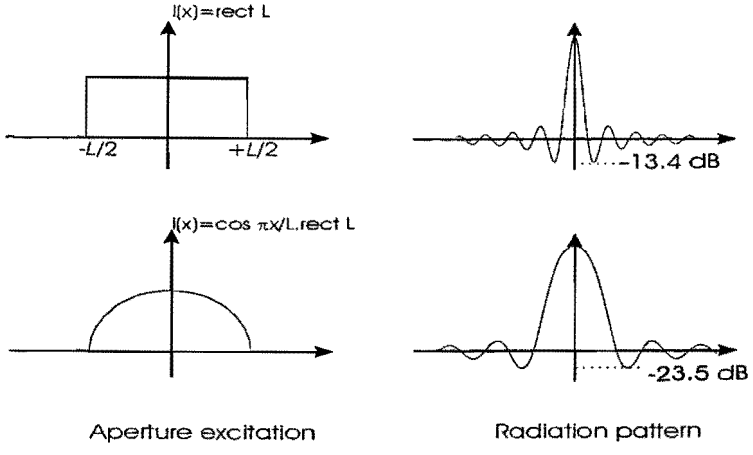

Figure 2.6. Visual representation for two current distribution functions and their corresponding radiation patterns.

2.3 The requirements for SKA

As mentioned in the introduction, SKA should not only have a very high sensitivity and an extremely fine resolution, but also a broadband behaviour. This requires an over-all large physical size in terms of wavelength. If a uniformly spaced array fulfilling the criteria (2.11) at the highest frequency, is employed, a large number of elements is needed. In the case of SKA, consisting of 32 circular stations each of a diameter of 300 meters, the number of elements required in a equivalent uniformly spaced array operational at the highest frequency will be approximately 12 million of elements per station which is 12 times the estimated value [1].

To reduce the number of elements, several techniques have been developed. All of these result in arrays with unequally spaced elements, also called aperiodic arrays. Aperiodic arrays match the requirements pursued by SKA: a broadband behaviour, without grating lobes and with a low side-lobe level. The literature gives a huge amount of design procedures that result in aperiodic arrays. Based on the requirements for SKA, we have pointed out three design procedures in the next Chapter.

Chapter 3

Literature review of aperiodic arrays

In the previous chapter, we have presented the parameters used to describe an array. In this chapter, we present possible solutions given in the literature which address the problems raised by SKA. The solutions should suppress grating lobes and keep a low side lobe level.

We have focused our attention on three types of design procedures. In the first part, we present density taper methods. The second part points out techniques based on rotations. Finally, in the third part we present random arrays.

3.1 Density taper designs

3.1.1 Introduction

The first significant work on non-uniformly spaced arrays was carried out by Unz [3]. Since that time a large number of contributions have been made to this field. King *et al.* [4] computed the pattern functions of a few sample arrays with prearranged spacings. Their computed results revealed some interesting properties of non-uniformly spaced arrays:

- an antenna array with unequally spaced elements needs fewer elements than an equally spaced array to suppress grating lobes;
- the suppression of the grating lobes can lead to a high side-lobe level.

Non-uniformly spaced arrays were also studied by Swenson *et al.* [5] at the University of Illinois in connection with the feed of a radio telescope. A new design technique, based on both variable spacing and variable excitation, was established. In this technique the element spacings are related to an excitation function as is usually referred to a class of design called ***density tapering***. This technique is inspired by

amplitude taper methods, used with continuous antenna apertures. In amplitude taper procedure, the illumination of a continuous aperture is tapered so that the received energy is larger at the centre than at the edge. It results in the possibility to achieve low side lobes by using a proper taper function. See Table 3.1 for the side-lobe levels achieved with various tapering functions. Density taper designs based on the approximation of the amplitude taper illumination function of a continuous aperture. The signal at each element of the array is of equal amplitude but the spacing between adjacent elements differ. Thus the density of equal-amplitude elements varies as a function of location within the array. By analogy to the amplitude taper, the equal-amplitude elements will be, in general, more dense at the centre of the array than at the edge. As soon as there is no periodicity in a density-tapered array, grating lobes disappear.

Type of amplitude taper	Level of the highest side lobe (dB
Rectangle	-13.4
Circle	-17.5
Parabola	-22.3
Cosine	-23.5
Triangle	-26.8
Raised Cosine	-32.1

Table 3.1. Different types of functions used for tapering the amplitude of the aperture and the corresponding side lobe level [15].

There are two basic design approaches to match a density taper to an amplitude taper. In the one technique the density is matched deterministically to the desired amplitude taper by certain approximation techniques applied to the integral of the aperture illumination. The other design technique is a statistical method which utilizes the desired amplitude illumination as a probability density function for determining whether or not an element should be located at a particular point within the array aperture [7].

3.1.2 Statistical density taper

For the statistical method we refer to the work of Willey [6] and Skolnik [7]. In this approach, the density of elements located within a given aperture is made proportional to the amplitude distribution of the conventionally "filled" array. Skolnik removes elements from a regular grid defined by a minimum spacing; the selection of the element locations is performed statistically by utilising the amplitude taper as the probability density function. Let us describe this approach.

The method starts off with a uniformly filled array with the minimum allowable inter-element spacing. We consider here a circular planar array as shown in Figure 3.1. Its elements are placed on a regular grid and are defined by their polar

coordinates r_m and θ_m , where $r_m \in [0,1]$, is the normalized radial coordinate of element m. The m^{th} element of the filled array has a constant amplitude $F(r_m)$. We can write the expression for the far-field as follows,

$$E(u,v) = \sum_m F(\vec{r}_m).e^{j\vec{k}.\vec{r}m} \qquad (3.1)$$

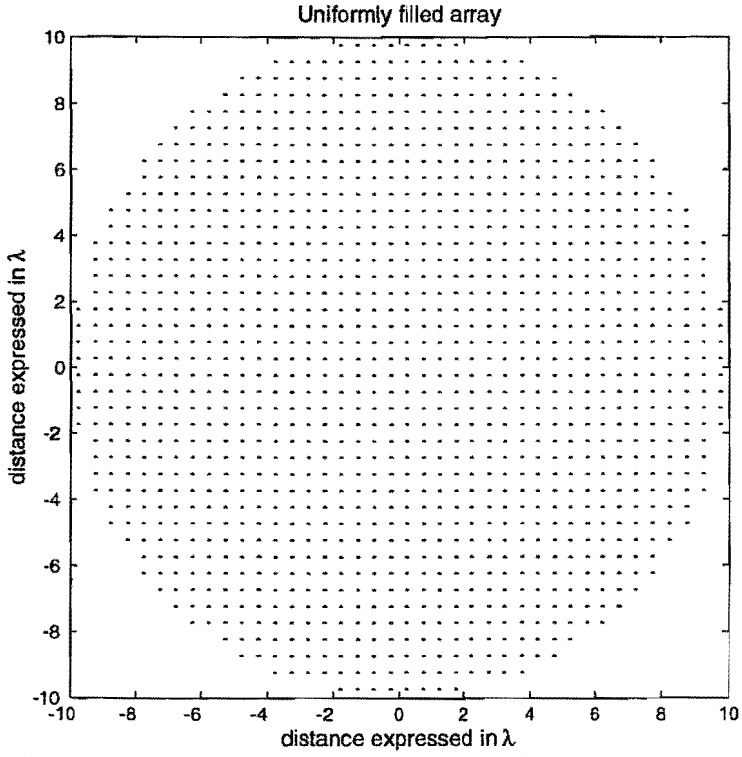

Figure 3.1. A uniformly filled array with 1264 elements.

The thinning procedure is the following. We use a raised cosine-squared function as the amplitude taper function $A(r)$ (see Figure 3.2). Let $U(m)$ be a random number uniformly distributed between zero and one, and let k be a thinning factor (in this example we use $k = 1$). We determine whether or not the m^{th} element will be removed ($F(r_m)=0$) if $U(m) \geq kA(r_m)$; otherwise $F(r_m)=1$.

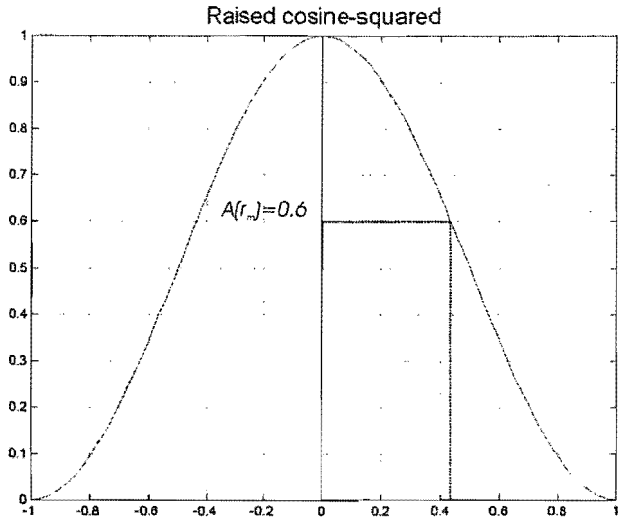

Figure 3.2. The amplitude taper function used as probability density function in the thinning procedure.

Elements located near the centre of the array are on average more likely to remain than elements near the edge. For example, an element located at $r = 0.42$ will be maintained with a probability of *60 %*. The thinning procedure has been applied to the filled array presented in Figure 3.1 with the amplitude taper model shown in Figure 3.2. The resulting array is shown in Figure 3.3.

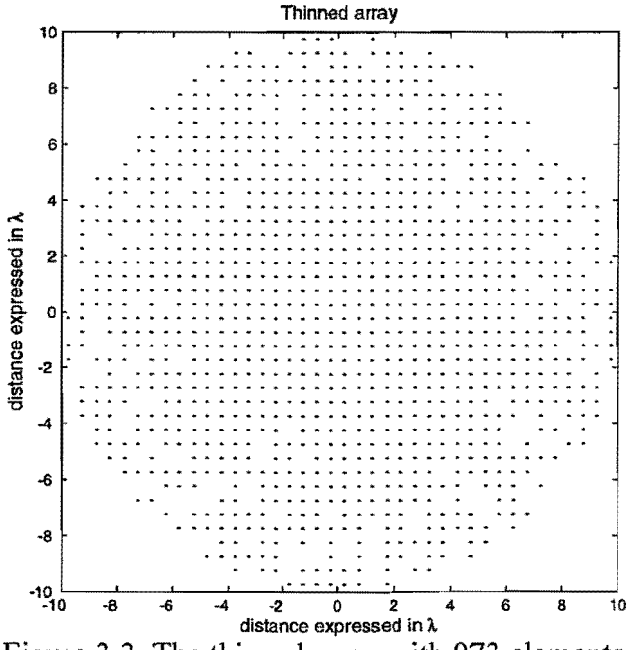

Figure 3.3. The thinned array with 973 elements.

In the array presented in Figure 3.3, *23 %* of the antenna elements of the filled array have been removed. The number of removed elements can be controlled by the thinning coefficient k and also by the type of amplitude taper function. A thinning coefficient smaller than one, will result in an array with fewer elements.
The choice of the amplitude function affects not only the number of elements but also enables the designer to control the level of the near-in side lobes. Figure 3.4a and 3.4b show respectively a u-cross section of the radiation pattern of the filled array and the thinned array.

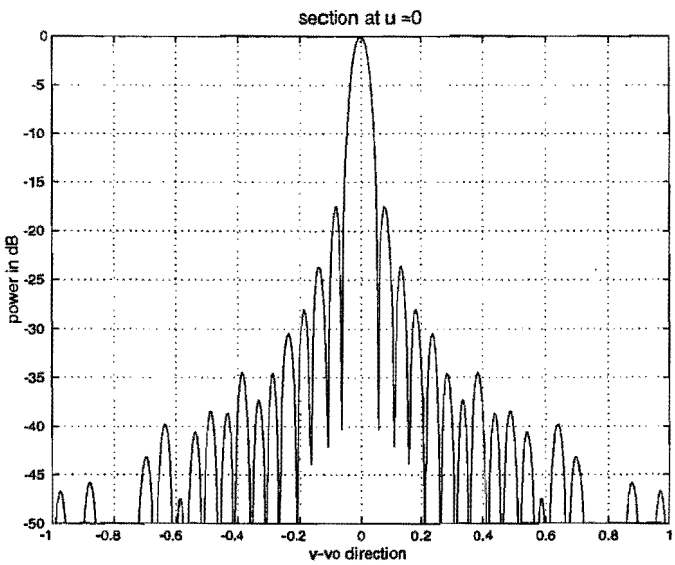

(a)

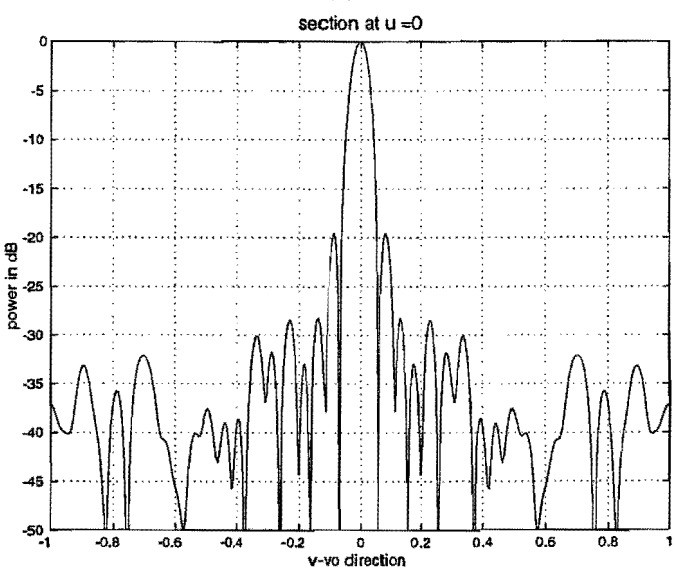

(b)

Figure 3.4. u-cross-section of the radiation pattern. (a) The *1264*-element filled array. (b) The *973*-element thinned array.

The average power pattern of a thinned (see [7] for a detailed proof) can be expressed as follows,

$$\left\langle \left|E(u,v)\right|^2 \right\rangle = k^2 \left|E_0(u,v)\right|^2 + \sum_m kA_m(1-kA_m) \qquad (3.2)$$

where A_m is the normalized amplitude of the excitation that would be applied to the m^{th} element of the conventional amplitude-tapered antenna with a field intensity of,

$$E_0(u,v) = \sum_m A_m e^{j\vec{k}\vec{r}} \qquad (3.3)$$

The first term of Equation (3.2) is proportional to the radiation pattern of the model amplitude-tapered array. The second term is independent of angle. Thus the average side-lobe level which dominates the pattern outside the vicinity of the main beam may be written as

$$\overline{SL} = \sum_m kA_m(1-kA_m) \qquad (3.4)$$

Skolnik [7] shows that the level of the near-in side lobes is approximately the same with the thinning procedure as with an amplitude taper technique. This can be shown using Equation (3.2). The major portion of the radiation pattern is governed by the statistical side lobes, with an average value given by Equation (3.4). This equation shows that the statistical side-lobe level of a thinned array is determined by the amplitude taper function A, used as probability density function, and by k, the factor which determines the number of elements removed. Skolnik also shows that the shape of the main beam is relatively unaffected by the removal of elements, as it can be seen in Figure 3.4.

As with any statistical process, there must be enough "samples" to ensure statistical regularity. Hence the statistical density taper design requires that the array contain a sufficient number of elements. It has been found, empirically that arrays of more than 100 elements are probably adequate for applying this technique.

The thinning procedure was extended by Mailloux and Cohen [8]. They utilised the statistical thinning of arrays with quantized element weights to improve the side-lobe performance in large circular arrays. Their results demonstrated the possibility to obtain considerable side-lobe reduction by a combination of probabilistic thinning and discrete amplitude quantization. Figure 3.5 shows an example of an array obtained by Mailloux and Cohen.

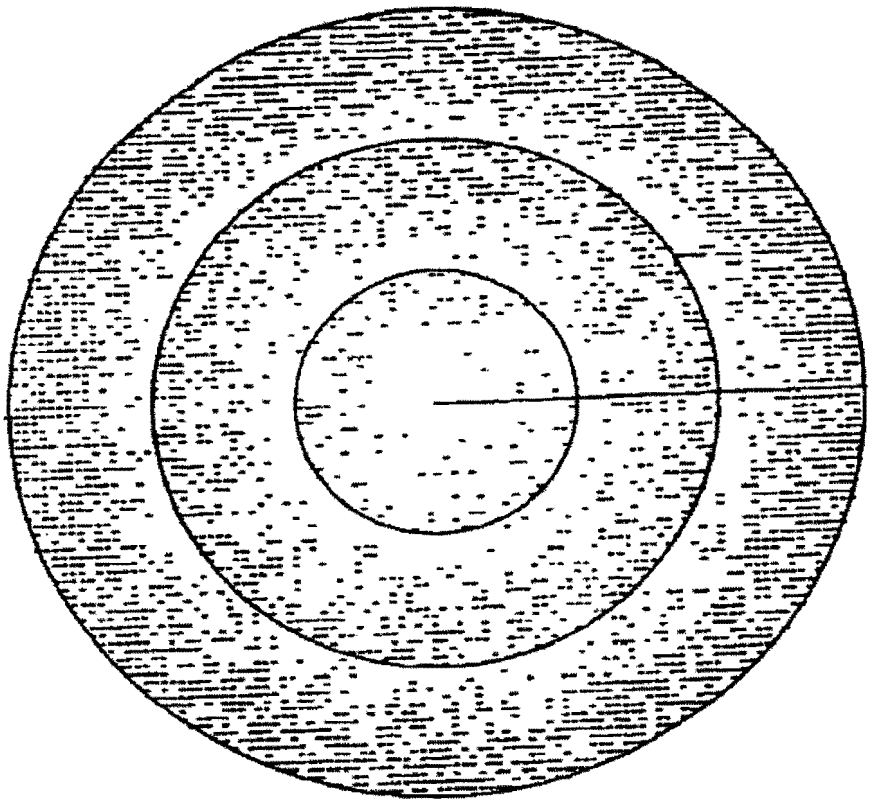

Figure 3.5. Example of an array obtained by the technique of Mailloux and Cohen [8].

The thinning procedures, established by Skolnik [5] or by Mailloux and Cohen [8] are interesting for their manner to control the side lobes. Close to the main beam we can predict the level of the side lobes. However, the elements still have to be positioned on a regular grid, which means that if the inter-element spacing of this underlying regular grid exceeds half a wavelength, grating lobes appear. This point is a serious limitation for the broadband behaviour that we have expected for this kind of configuration. In the case of SKA, the inter-element spacing at the highest frequency should still be *7.5 cm* if we want to avoid grating lobes. If we satisfy this condition, we may still expect the number of elements after thinning to be too expansive.

The other main drawback of this class of design is the extreme difficulty of the mutual coupling analysis. In a mutual coupling analysis, the presence of symmetries in a large array is essential to reduce the computation time. However, in thinned array, the neighbourhood of each antenna element varies along the array, and a mutual coupling analysis will be computationally prohibitive.

3.1.2 Deterministic density taper

Maffett [9] has proposed the same deterministic method as Swenson *et al.* [5] to relate the element position of a linear array to the amplitude function. The case of a planar array is more involved. We will see in Chapter 4 how to perform a proper density taper with a planar array. In Chapter 4 we also give a straightforward presentation of the deterministic density taper method.

3.2 Rotation designs

3.2.1 Ring arrays

Holst and Dennis [10] developed a technique to avoid the grating lobes and reduce the side-lobe level by changing the arrangement of the elements in a circular antenna array. The centres of the antenna elements are located in respective concentric rings about a centre element in each ring being equally spaced and arranged asymmetrically with respect to the centres in the other rings. Figure 3.6 shows the array obtained with the Holst method. The positioning of the elements produces a randomness in behaviour with respect to the grating lobes, with the effect that the grating lobe energy is smeared across the side-lobe pattern.

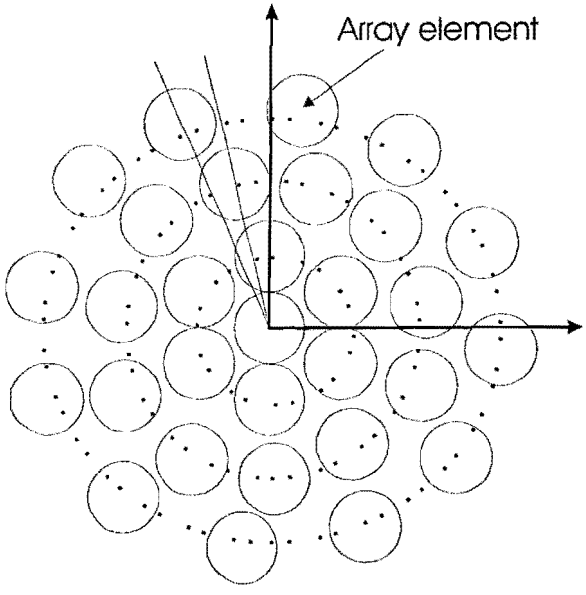

Figure 3.6. An array with 49 elements obtained with the Holst method [10]. Each circle represents an array antenna element.

This approach is generalized in the method used by Kaploun [11]. Kaploun places the array elements along several rings, which results in a configuration with a quasi-

random distribution. The choice of the number of elements in each ring enables the designer to optimize the average side-lobe level. We invite the reader to consult the work reported in reference [11].

In the approaches of Holst and Kaploun the underlying idea is a density taper applied to a circular array. This density taper is both a radial and an azimuthal taper. This means that the distance between the rings varies, the radius from the inner rings to the outer rings increases; and the angle between elements from one ring to another vary in the same manner as previously. In Chapter 4, we apply various radial density taper methods to circular arrays. We end up with results that are similar to the configuration of Holst and Kaploun.

3.2.2 Rotation of subarrays

Another method to suppress the grating lobes is based on rotations and has been proposed by Agrawal [12]. In this method a regular array with uniformly spaced elements is split into subarrays, and then each subarray is rotated by a specified angle, as seen in Figure 3.7. As a result, the grating lobes, which remain at the same angular distance from the main lobe, are multiplied in number by the number of subarrays while their amplitude is divided by the same number.

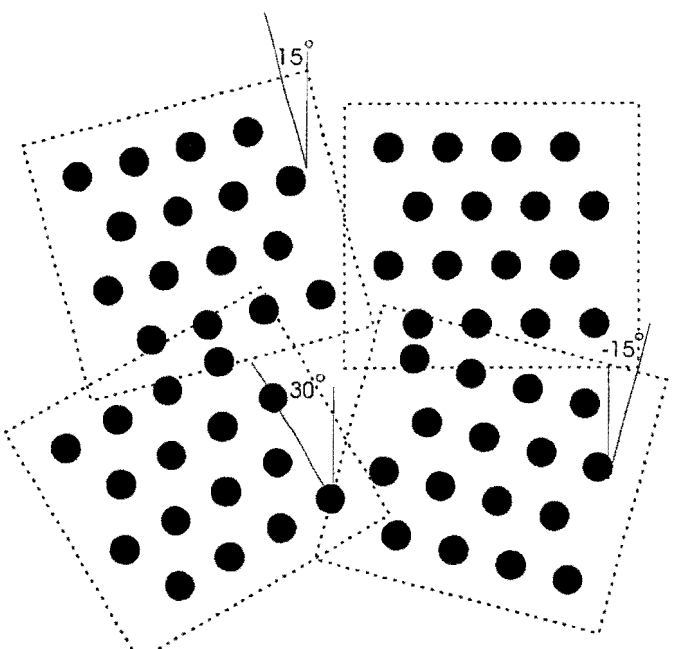

Figure 3.7. A *64*-element array consisting of four subarrays rotated by 0°, 15°, 30°, and -15°, respectively.

Figure 3.7 shows a *64*-element array obtained with the technique described by Agrawal [12]. The original array had 8×8 elements arranged in a triangular lattice. This array was divided into four subarrays each containing 16 elements. The subarrays were rotated by by 0°, 15°, 30°, and -15°, respectively. The value of the

rotation angle α is a design parameter determined by the geometry of the original array. Agrawal established that α is independent of frequency.

The computation of the radiation pattern of the Agrawal array shows that the grating lobes effectively disappear but the level of the nearest side lobes is still around *−11* dB. Agrawal predicted the level of the side lobes; it is directly linked with the number, *n*, of subarrays used. The amplitude of the main beam of the *n* subarrays are added up while the amplitude of their grating lobes are juxtaposed. So, for a given *n*, the side lobes will be *20 log(n)* dB below the main beam. Thus, the value of *11* dB must be related with the expected value of $20\log(4) \approx 12$ dB.

3.3 Random arrays

3.2.1 The two types of random array

A random antenna array is one type of aperiodic array. It is a sparse (or thinned) array in the sense that the inter-element spacing is larger than $\lambda/2$. Its elements are positioned at random over the array aperture according to a given probability distribution. Different kinds of probability distributions can be applied to determine the element locations.

The first type of random array, described by Lo [13], is completely random. These arrays consist of array elements that are distributed independently and according to the same probability distribution across a common area. This type of random array was considered by Lo [14] in early papers on the subject and is treated extensively in Steinberg's book [15].

The second type of random arrays satisfies a nearest-neighbour constraint and was discussed by Fante *et al.* [16]. Fante analysed the effect of a nearest-neighbour constraint on the radiation pattern of a large, circular, random array. This constraint prevents elements to be positioned too closely to each other and allows for the reduction of the mutual coupling between the elements.

3.3.1 Unconstrained random arrays

A theory developed by Lo [13] describes this kind of random array where the elements are equally excited and placed at random within an aperture in accordance with a common probability density function, *g(X)*. We give in this part the major results established by Lo:

- The mathematical expectation of the radiation pattern.
- The average side lobe level (SLL).
- The critical number of elements, *N*, to achieve a certain side-lobe level with a given probability of success.

In the following discussion, all the length dimensions are normalized to the wavelength . For simplicity a linear array of length a is considered first. Let $g(X)$ be the probability density function to place an element at X, with $|X| \le a/2$ and

$$\int_{-a/2}^{a/2} g(X)dX = 1. \qquad (3.5)$$

All N elements of the array are placed according to this probability function but independently from each other. For each set of random samples $\{X_n\}$: $(X_1,X_2,...,X_N)$ there is an associated a sample pattern function,

$$E(u) = \frac{1}{N}\sum_{n=1}^{N} e^{jux_n} \qquad (3.6)$$

where x_n is the normalized element position. The mathematical expectation of the sample pattern function, one obtains

$$\begin{aligned} \langle E(u) \rangle &= N\left\langle \frac{1}{N} e^{jkux} \right\rangle \\ &= \left\langle e^{jkux} \right\rangle = \int_{-\infty}^{\infty} g(x) e^{jkux}\, dx \end{aligned} \qquad (3.7)$$

Equation (3.7) shows that the relation between the pattern function, $\langle E(u) \rangle$, and the aperture excitation is a Fourier transform. So, there is no difficulty to choose a proper probability density function $g(x)$ which will yield at least a desirable mean pattern. Let us call this desired mean pattern $E_0(u)$. It is related to some continuous current density $i_0(x)$, by the far-field transformation relation

$$E_0(u) = \int_{array} i_0(x) e^{jkux}\, dx \qquad (3.8)$$

Normalisation of $E_0(u)$ by setting $\int_{array} i_0(x)dx = 1$ gives the interesting relation,

$$g(x)=i_0(x) \text{ implies } \langle E(u) \rangle = E_0(u)$$

This relation implies that the average, complex radiation pattern can be matched to any radiation pattern that is derivable from a real current density by selecting the probability density function of the element location according to the latter equation.

The power pattern of an array is the product of the radiation pattern, $E(u)$, and its complex conjugate. It may be written

$$\left\langle |E(u)|^2 \right\rangle = |E_0(u)|^2 \left(1 - \frac{1}{N}\right) + \frac{1}{N} \qquad (3.9)$$

This equation consists of two terms. The first term is the desired power pattern, slightly reduced by the second term. The second term of strength *1/N*, is the **average side lobe level,** and angle-independent. The presence of this term implies that the designer has only limited control over the side-lobe region. As an example, consider a probability density function

$$g(x) = \begin{cases} \cos^2(\pi x/2) \; for \; |x| \le 1 \\ 0 \qquad\qquad otherwise \end{cases}, \qquad (3.10)$$

Figure 3.8a shows the layout of a random array created with this probability density function. The expected power pattern, $|E_0(u)|^2$, for this kind of distribution has its first side lobes at *–32* dB as we have shown previously, in Section 3.1.1. In Figure 3.8b, we have plotted the theoretical radiation pattern of the circular random array depicted in Figure 3.8a.

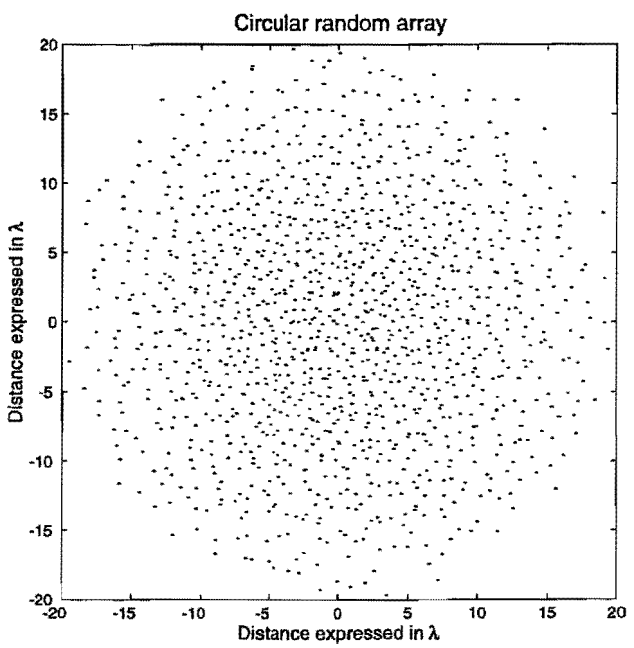

(a)

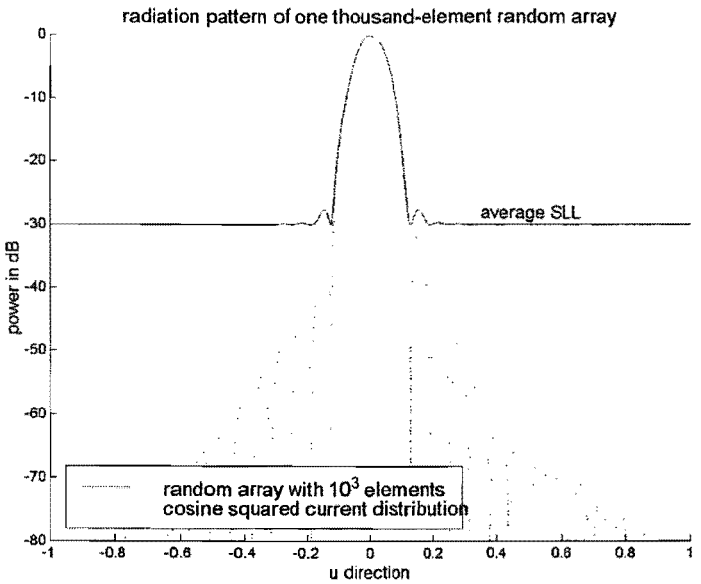

(b)

Figure 3.8. (a) Layout of the circular random array of *1000* elements. (b) In solid line, its corresponding average radiation pattern (RP). In dot-dashed line, RP of the equivalent continuous antenna tapered by a cosine squared current distribution.

The first side lobe of the amplitude tapered array is at –32 dB and the side-lobe level decreases monotically with angle. The solid curve shows the power pattern of the linear random array. The side-lobe level (SLL) remains at *–30* dB, as expected form Equation (3.9).

Once the number of elements has been chosen, it is not guaranteed to achieve a prescribed side-lobe level. Indeed, this level fluctuates around an average of *–10log(N)* dB. Lo [14] has established a relation that links the critical number of elements to achieve a certain side-lobe level with the chance of success, say *80 %—95 %*. A graph illustrating this relation is available in [13]. From this graph, the required number of elements associated with a certain side-lobe level can be determined for a given probability and an expected aperture size. It should be understood that this procedure is a systematic design procedure. A disadvantage of this design procedure is that strong mutual coupling occurs as soon as the array elements are closely spaced. This problem is overcome by the nearest-neighbour constraint method developed by Fante *et al.* [16].

3.3.2 Random array with a nearest-neighbour constraint

A nearest-neighbour constraint enables the designer to set a minimum allowable spacing between an array element and its nearest neighbour. As previously, for the sake of simplicity, we consider a linear array of length, L, and N array elements. The probability density function of an element x_l is $p(x_l) = 1/L$, for $-L/2 \leq$

$x_1 \leq L/2$, and $p(x_1) = 0$, otherwise. With the nearest-neighbour constraint, the conditional probability function, $p(x_2/x_1)$, of an element x_2, for a given x_1, must have the form shown in Figure 3.9.

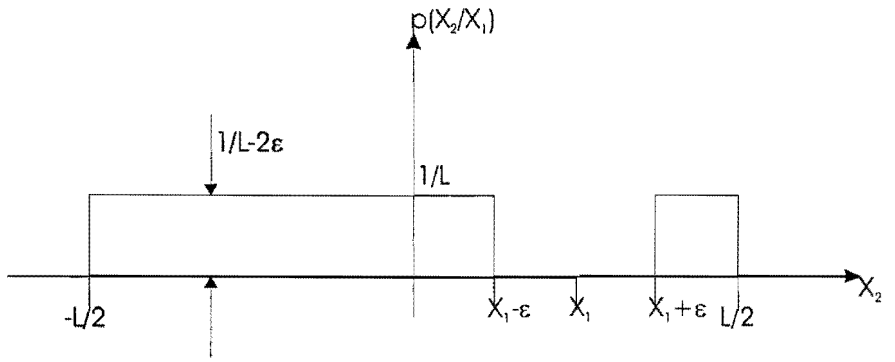

Figure 3.9. Conditional probability density $p(x_2/x_1)$ of an element x_2, for a given element, x_1, with a nearest-neighbour constraint.

Thus element x_2 can be positioned anywhere, except in the excluded region of width 2ε around x_1. By taking into account the nearest-neighbour constraint, the average expected power pattern is [16]:

$$\left\langle |E(u)|^2 \right\rangle = |E_0(u)|^2 \left(1 - \frac{1}{N}\right) + \frac{1}{N}\left[1 - f\,\mathrm{sinc}(ku\varepsilon)\right] \qquad (3.11)$$

where sinc is a sinus-cardinal, and f is a measure of the element density defined by,

$$f = \frac{2\varepsilon(N-1)}{L} \qquad (3.12)$$

Equation (3.11) is similar to Equation (3.9). Here $|E_0(u)|^2$ is the radiation pattern of a continuous linear array of length L. The second term in Equation (3.11) represents the average side-lobe level, modified by the constraint on nearest neighbours. Equation (3.11) is depicted in Figure 3.10. Near the main lobe, the side lobes decrease drastically to a level of $(1-f)/N$. However, for $u \geq \pi/k\varepsilon$ the side-lobe level reaches its average of $1/N$.

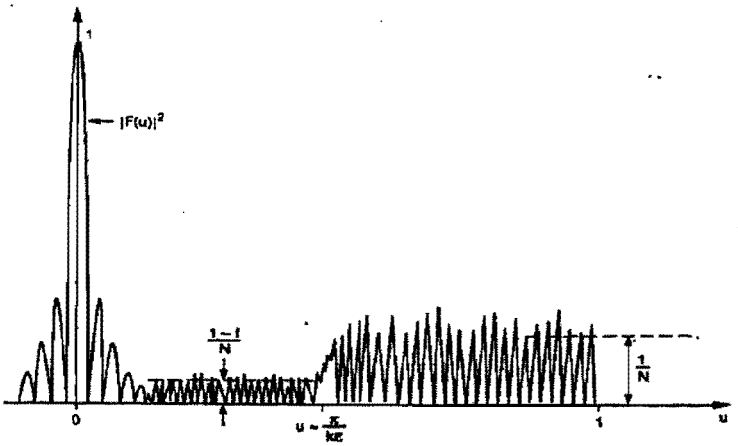

Figure 3.10. Graphic representation of Equation (3.11), [16].

The designer can use the width 2ε as a design parameter for this type of array. But there are some limitations on the value of ε. Indeed in Equation (3.11), the second term can be negative which is physically impossible. If we call the average spacing between the elements of the array $\langle d \rangle$, then the length, $L \approx (N-1)\langle d \rangle$ and $f = 2\varepsilon/\langle d \rangle$. f decreases as the reciprocal of the average spacing $\langle d \rangle$ and there is no problems; however the near-in side lobe will not be reduced anymore. When f increases, $\langle d \rangle$ decreases to a minimum value of 2ε and cannot exceed this threshold for physical reasons. In the case of SKA, this limitation will not be a disadvantage because it enables to place the elements far away from each other in terms of wavelengths and reduces the mutual coupling.

3.3 Conclusion

Three types of design approaches were identified in the literature that could be of interest for the design of SKA: designs based on density taper, on rotations and on randomization. All of these methods suppress the grating lobes and achieve low side-lobe level.

Density taper method and random procedure have the advantage to provide the designer with control parameters. The designer can control the shape of the main beam and the near-in side-lobe level by the proper choice of either an amplitude taper function or a probability density function used to place the array elements. However, statistical procedures were found to be limited since strong mutual coupling can occur. A random array satisfying a nearest neighbour-constraint has the advantage to prevent elements from lying too close to each other and reduce, at the same time, these mutual coupling effects.

Approaches based on rotations also suppress the grating lobes but do not lead to a systematic design procedure. Once the number of subarrays has been chosen the shape of the main beam and the side-lobe level cannot be predicted.

Chapter 4

Application of the literature review

In the previous chapter, we have identified three techniques that could be applied for the design of SKA. In this chapter, we present three classes of arrays inspired by these techniques. The first class will be called hexagonal-logarithmic-rotated-subarray array, the second one regular-perturbed array and the third one radial-density-tapered array.

To design the classes of arrays, we developed software. In Section 4.2 to 4.4, we present the hexagonal-logarithmic-rotated-subarray array, the regular-perturbed array and the radial-density-tapered array, respectively.

4.1 Structure of the software

4.1.1 Specifications

In order to analyze different types of arrays, we developed user-friendly software that calculated the radiation pattern of an array. The software must give the possibility to design an array from its parameters or from the location of its elements given as an input. For instance, for a regular array, the number of elements per row and column and their spacing should be sufficient for its design. The software should also provide specific options for the visualization of the radiation pattern. In particular, cross-sections in the u- or v-directions should be possible. It should also offer the possibility to change parameters of the computation, like the frequency.

4.1.2 Structure

Based on the specifications mentioned previously, we have decided to program the software in MATLAB® because it is one of the few and best applications available for providing both computational capabilities and data displaying in a variety of graphical representations. Moreover, specific MATLAB packages allow matrix computation and, sophisticated graphics and graphical user interfaces.

4.1.2.a Main program

We have programmed a graphical user-interface (GUI) called *ArrayBuilder*. This GUI is the root of our software. It presents four main parts and three additional buttons. The largest part in term of space is a frame where graphics are displayed, the second, third and forth parts correspond to the pop-up menus. Those pop-up menus correspond to the requirements defined above; they are named *Type of array, Visualization,* and *Options*. The three buttons *Plot, Compute* and *Close* carry out respectively the display of an array in the main frame, the computation of the radiation pattern and the closing of the window. Figure 4.1 shows the structure of the GUI *ArrayBuilder* and Figure 4.2 presents its general layout.

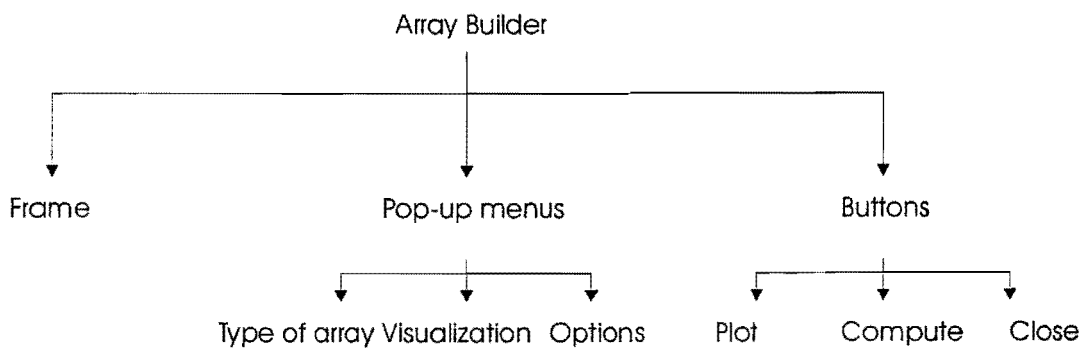

Figure 4.1. Structure of the main program *ArrayBuilder*.

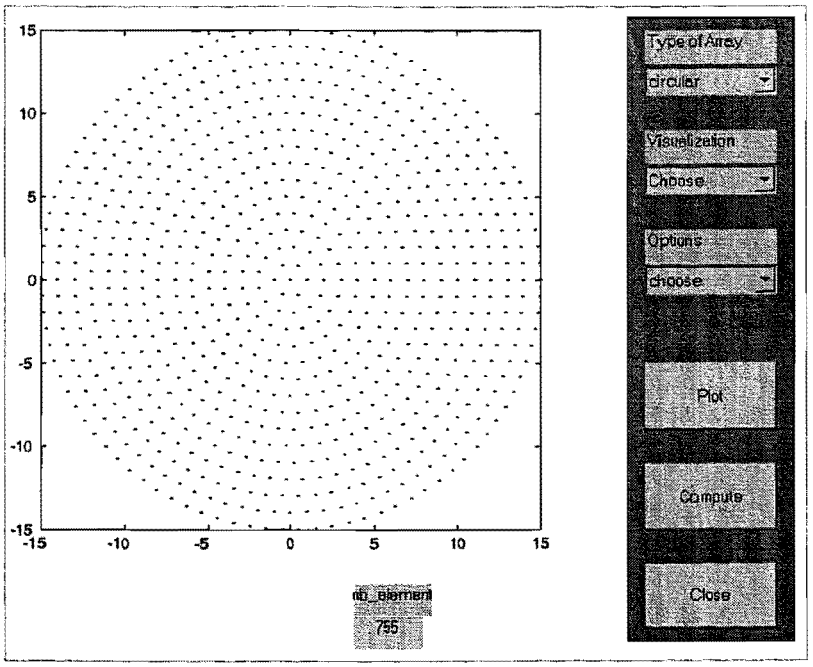

Figure 4.2. General layout of the GUI, *ArrayBuilder*.

4.1.2.b Pop-up menus

- *Type of array*

This menu is divided into five options. All these options are related to the definition of the arrays. There are two types of options: the first type of option needs parameters to design an array whereas the second type of option has predefined array element locations. When you click on an option of the first type, a new window appears where the user has to set the characteristic parameters of an array. Figure 4.3 presents the structure of the pop-up menu, *Type of array*.

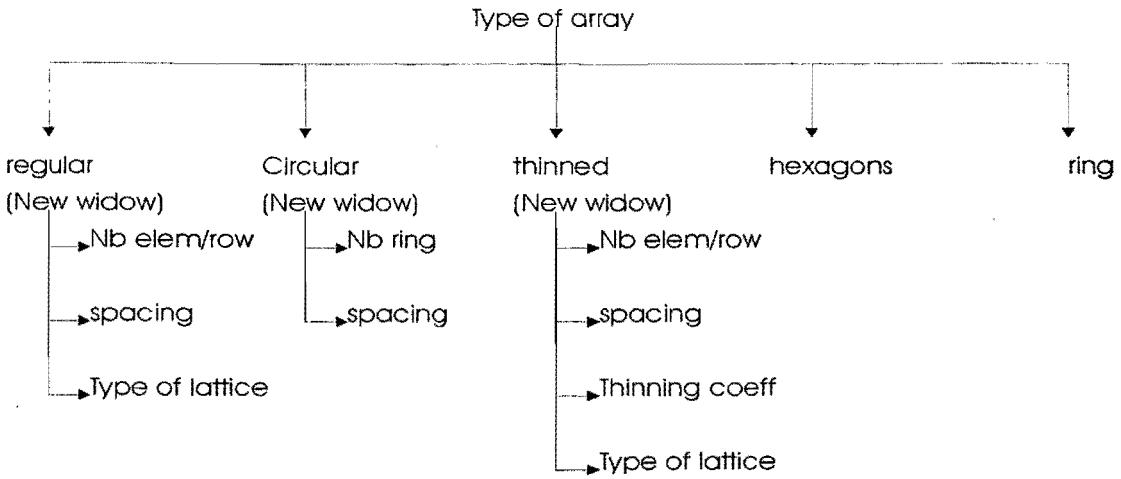

Figure 4.3. Structure of the pop-up menu, *Type of array.*

Before going further in the description of the two other pop-up menus, we have to explain how we have defined the parameters for the *regular, circular* and *thinned* arrays.

A *regular array* is defined by its *number of elements* per row and per column, its inter-element *spacing* and its type of *lattice*, which can be either *rectangular* or *triangular.* In the module corresponding to the regular array, the user has to set these parameters. In the software, we should note that the number of elements per row equals the number of elements per column.

The *circular array* is defined by its *number of rings* and the *spacing* between two elements of the same ring. The spacing between two rings is equal to the inter-element spacing within a ring. The user is free to improve the soft, and can define a circular array with more than these two parameters.

The *thinned array* is obtained after thinning a circular array that has a regular (rectangular or triangular) underlying grid. For this reason, the user first sets parameters corresponding to a regular array. Then, a circular shape of the regular array is taken, and finally the thinning procedure is applied. Thus the *'number per row'* parameter corresponds to the number of elements lying along the horizontal diameter. The user also has to specify the inter-element *spacing* and the *type of lattice* of the underlying grid. After that, the user chooses the thinning procedure to be applied. At this stage, the interface offers the possibility to change the thinning coefficient. Further developments may consist of defining different amplitude taper illumination functions.

The *hexagon* and *ring* options correspond to arrays with predefined element locations. *Hexagon* stands for the hexagonal-logarithmic-rotated-subarray array, which is studied in Section 4.2.3. *Ring* stands for an array composed of rings, but it is not presented in this report.

- *Visualization*

This menu is divided into three options, called the u-u_0 *section,* the v-v_0 *section* and *viewer3D*. The first two options allow cross-sections along the u or v-planes of the three dimensional radiation pattern of an array. To perform such a section, one has to define the direction expressed in terms of u or v where the section is desired. The last option, *viewer3D*, is very useful to determine which aspect angle provides the information to be conveyed.

- *Options*

This pop-up menu is divided into four options named *average spacing, perturbation, density taper* and *precision.* The *average spacing* and the *precision* are two parameters used for the computation of a radiation pattern. The other two options act on the configuration of the array.

For a linear array, the average spacing is defined as the ratio between the length of the array and its number of elements. For a planar array, the inter-element average spacing is the square root of its area, divided by the number of elements. So, when the computation of the radiation pattern of a given array is started, to leave its average spacing unchanged, the parameter *average spacing* must be set to *1*. If this parameter is set to a value z, the average spacing of the array will be multiplied by the same factor z. It amounts to multiplying the size of the array by the same factor z. This parameter will be useful to test the broadband behaviour of an array.

In the software, the routine called *compute* evaluates the power pattern of an array by sampling the u-space and the v-space. The sampling is carried out with a certain step that corresponds to the *precision* of the computation. By default, the accuracy is set to *100*, which means that the u-space and the v-space are divided into *100×100* intervals for the computation. One should realize that a high accuracy, let say *200*, is time consuming.

The *perturbation* option introduces random perturbations on the array element locations (for more details, see § 4.3) and the *density taper* option applies a density taper to the array (see § 4.4).

4.1.2.c Buttons

The first button, *Plot*, displays the array defined by the parameters set with the pop-up menu *Type of array*. It also displays arrays that have been modified using the *perturbation* or a *density taper*.

The second button, *Compute*, computes and displays the radiation pattern. Two parameters are used for the computation, the coefficient for the *average spacing* and the *precision*.

Finally, the third button simply closes the window.

4.2 Hexagonal-logarithmic-rotated-subarray array

The starting point of our work was the study of a logarithmic array proposed by Craeye [17]. We will first present the characteristics of this type of array. One of its interesting features is its broadband behaviour. However, the broadband behaviour is obtained at the expense of high side lobes located on a cross. Therefore, we have applied techniques based on rotations in order to reduce this high side-lobe level.

4.2.1 Logarithmic array

The logarithmic array proposed by Craeye was chosen mainly for three reasons. It has a broadband behaviour over a frequency decade; no grating lobes enter the visible region; and structurally the array is attractive.

4.2.1.a Analysis of a linear logarithmic array

The array has a separable structure, which allows us to restrict our study to one dimension. Let us consider either a row or a column; the array will result from the multiplication of a row by a column. Along one row there are *16* elements split up into *4* clusters of *4* elements. Figure 4.4 shows the layout of one row. The inter-element spacings in each of these clusters are uniform but vary from one cluster to another. These spacings are expressed in wavelength and are respectively equal to *1* , *1.26* , *1.586* , and *2* , thus the total length of this array is roughly *11* . The variation of the spacing is relatively small because there is only a factor of *2* between the first and the forth cluster spacing. The average inter-element spacing for this *row*-array is determined by the ratio between the length of the row and the number of elements, i.e. *10.69 /16* $\approx$ *0.667* . A filled array of this length would require *22* elements. By using a logarithmic spacing, the number of element drops to *16*, which is *72%* of the number required for a uniform periodic array.

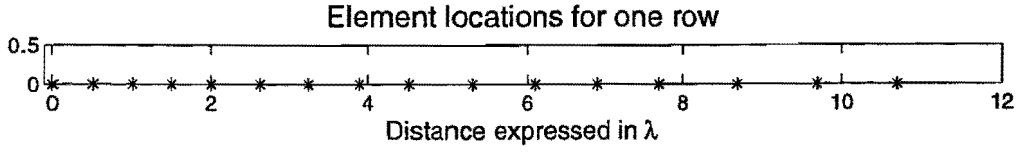

Figure 4.4. A *16*-element row of the logarithmic array.

Since this array is intended to have a broadband behaviour over a decade of frequency, we have computed its radiation pattern with an average inter-element spacing *(s)* running from one *0.667* to *6.67* .

When the average spacing is increased or decreased in the computation, the visible region is extended or restricted in a similar manner (see Section 2.1.2 and Section 4.1.2.b). A computation carried out with $\langle s \rangle = 0.667\ \lambda$ will focus on the main lobe, and the designer will be in a position to control the shape of the main lobe and the level of the near-in side lobes (the side lobes close to the main beam). A computation performed with $\langle s \rangle = 10 \times 0.667 \lambda$ will extend the visible region and will allow the designer to ensure that no grating lobes enter the visible region. Results are presented in Figures 4.5a, 4.5b, and 4.5c.

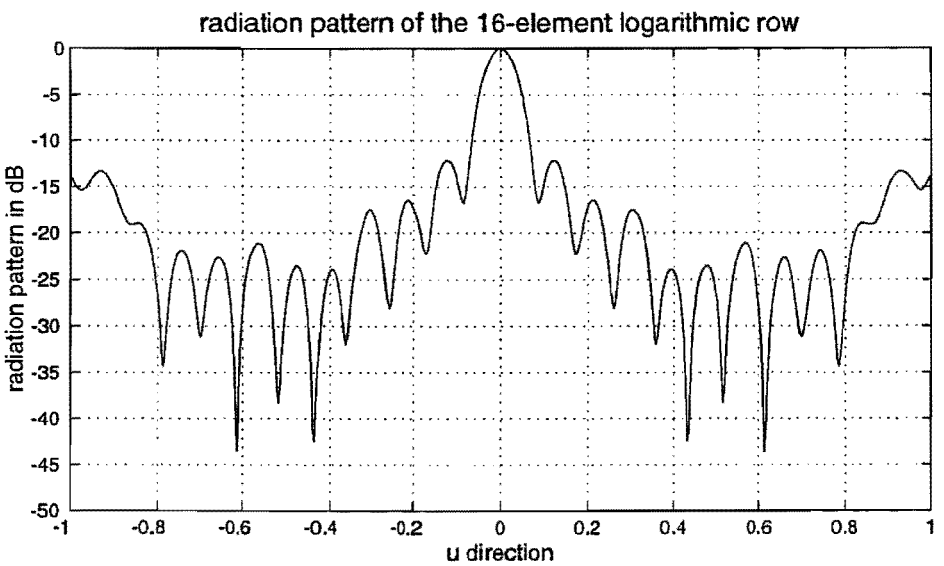

(a)

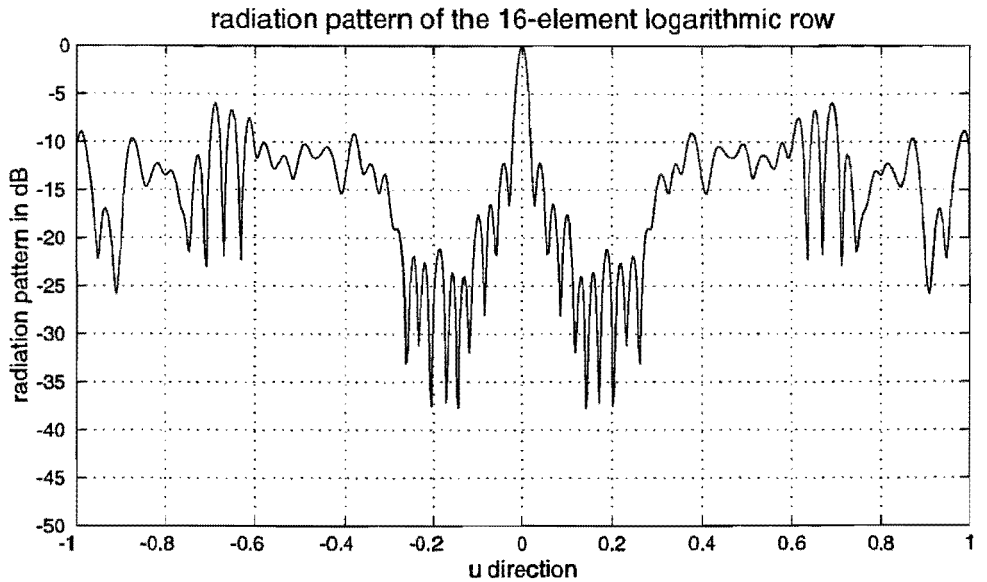

(b)

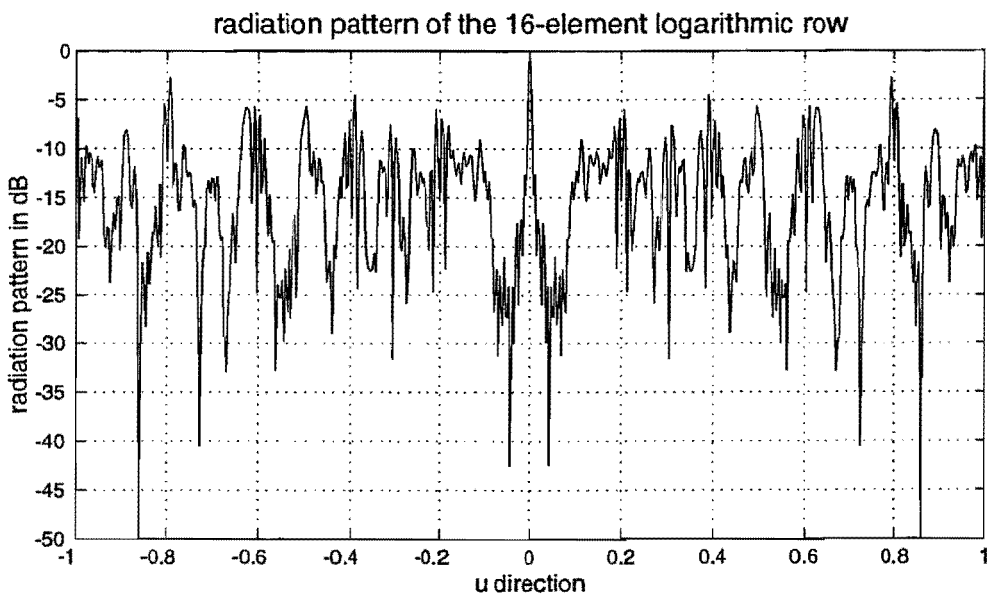

(c)

Figure 4.5. Radiation pattern of the *16*-element array. *(a) ⟨s⟩=0.667 λ (b) ⟨s⟩= 3×0.667 λ (c) ⟨s⟩=10×0.667 λ*

A close view of the main lobe is shown in Figure 4.5a. The level of the first side lobe is about *–12* dB and the side-lobe levels decrease monotonically to about *–22* dB at the forth side lobe. Figure 4.5b shows that beyond these four side lobes, a number of side lobes remain stable at around *–22* dB. Then the level rises sharply up to *–12* dB and stabilizes around this value. At high frequencies, which correspond to a high average spacing, Figure 4.5c shows a high variation of the average side lobes level with a peak side lobe at *–5* dB. Steinberg [15] shows that the distribution of phases at large scan angles tends toward a random distribution, and as a result, the distant side-lobe properties might be expected to be similar to those of a random array.

From these remarks, we can divide the radiation pattern into three regions. The first one comprises the main lobe and the near-in side lobes. Here the side lobes are controlled and remain relatively low. The next region is a transition region, in which the side lobe pattern degenerates toward that of the random array. The third region is composed of stabilized side lobes. Thus it was not surprising to remark that side lobes were stabilized at *–11* dB. It corresponds to the average side lobe level of a *16*-element random array (*-10log(16)=12* dB).

4.2.1.b The planar logarithmic array

Because of its separable structure, the logarithmic planar array results from the multiplication of a row and a column that we have studied. Rows and columns are identical in terms of structure and inter-element spacings. Figure 4.6a displays the general layout of the logarithmic array, and Figure 4.6b corresponds to its radiation pattern computed for an average inter-element spacing $\langle s \rangle = 3 \times 6.67$.

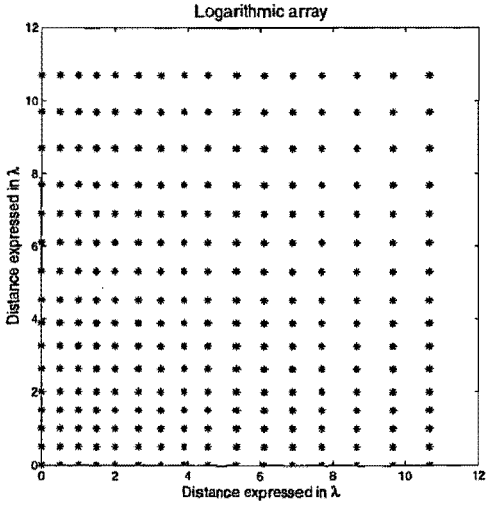

(a)

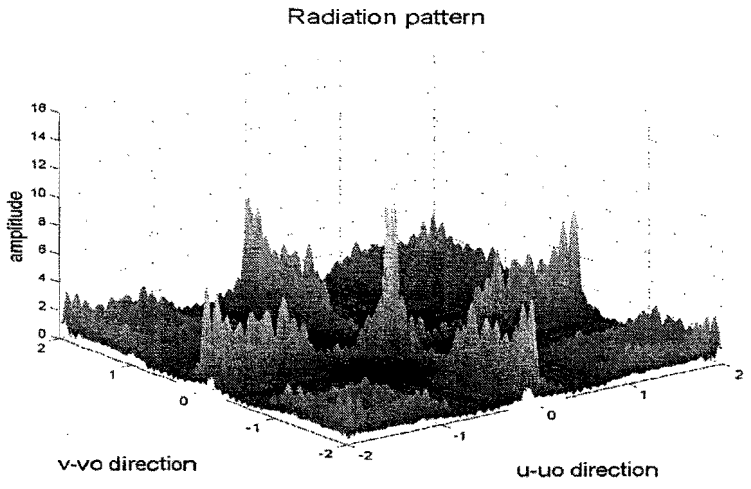

(b)

Figure 4.6. *(a)* Layout of the logarithmic array. *(b)* Corresponding radiation pattern computed for an average inter-element spacing $\langle s \rangle = 3 \times 6.67\ \lambda$.

The radiation pattern of the logarithmic array does not show grating lobes but relatively high side lobes, forming a cross in the *uv*-plane. This cross occurs due to the separable structure of the array. If we take a *u*- or *v*-cross section of Figure 4.6b we will obtain the same curve as the one shown in Figure 4.5b. It is interesting to notice that there is a factor of $1/N$ between the main lobe and the side lobes (N is the number of elements per row). For radio astronomy applications, the presence of this cross is a main disadvantage. Suppose that we steer the array to a weak distant source drowned in a neighbourhood of intense sources. The level of the cross is sufficient to enhance the intense sources up to a level comparable to the one of the weak source. To overcome this problem of high side lobes, a technique based on will be discussed below.

4.2.2 Logarithmic-rotated-subarray array

The main disadvantage of the logarithmic array is the presence of high side lobes lying along a cross in the *uv*-plane. In order to limit the influence of these side lobes, we built an array composed of logarithmic rotated arrays. A rotation of an angle, θ, in the spatial domain leads to a rotation of the same angle in the (u,v) domain. Thus, by an appropriate number of rotations n, the side lobes will smear out while the amplitude of the main lobe interfere constructively.

In order to smear out the side lobes in a regular manner, we have chosen a constant angle of rotation θ. This angle is defined by the desired number of rotations n and is bounded by $\pi/2$ (the cross has a $90°$ angle). From these remarks we can write

the angle of rotation as $\theta = \pi/2n$. The number of rotations n is also the number of subarrays required for the construction of the array. Figure 4.7 shows an example of logarithmic rotated subarrays, with $n=16$. In this example each subarray has the design of the logarithmic array that we have studied in Section 4.2.1. The total number of elements is *4096*.

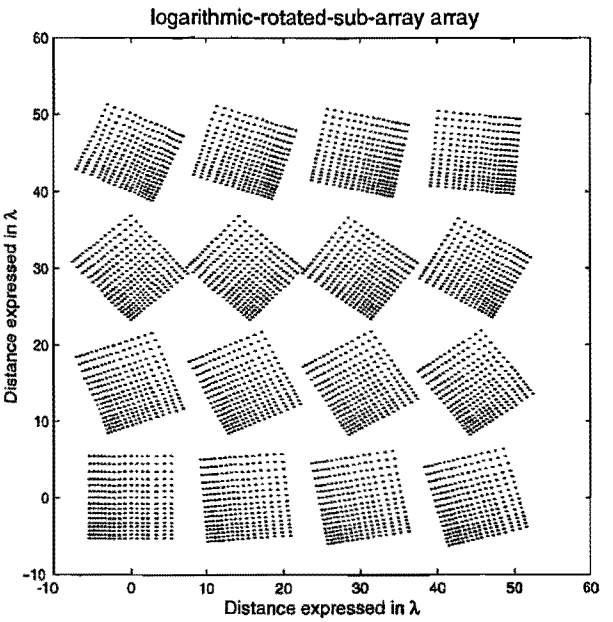

Figure 4.7. Layout of the logarithmic-rotated-subarray array

Distances are again expressed in wavelengths, and we find for the configuration an average inter-element spacing, $\langle s \rangle = 0.844\ \lambda$. In order to study the broadband behaviour for the array over a frequency decade, we have computed the radiation pattern for an average spacing at $1 \times 0.844\ \lambda$ and $10 \times 0.844\ \lambda$. The results are presented in Figures 4.8a and 4.8b.

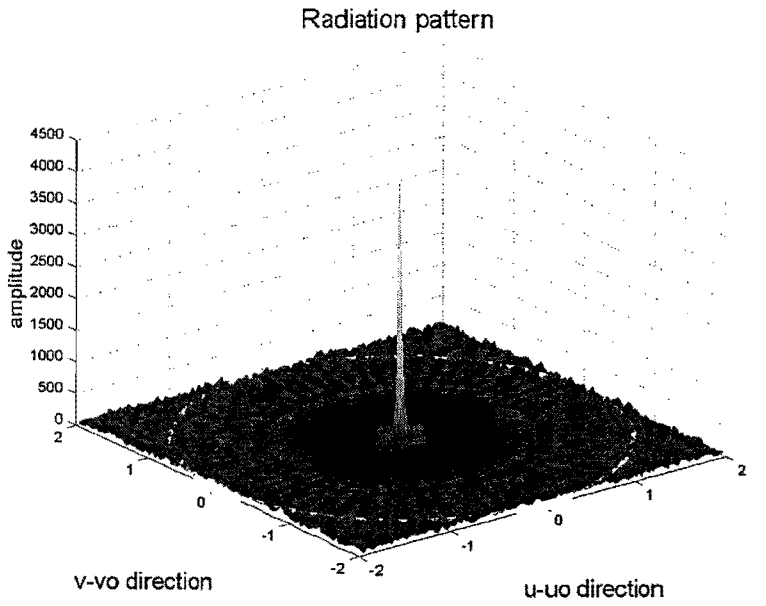

(a)

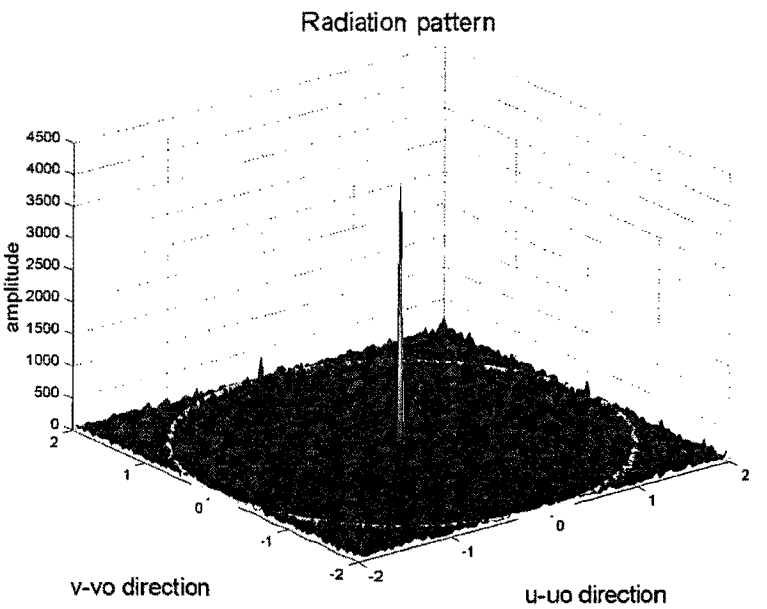

(b)

Figure 4.8. Radiation pattern of the logarithmic-rotated-subarray array with *4096* elements. *(a)* $\langle s \rangle = 1 \times 0.844\ \lambda$ *(b)* $\langle s \rangle = 10 \times 0.844\ \lambda$

Figure 4.8a clearly shows that the cross of the single array has been spread over the *(u,v)* space. A cross-section along the *u*-plane gives an average side-lobe level of *–35* dB, which corresponds to the value expected for a random array with the same

number of elements ($-10.log(4096) \approx -36$ dB). Figure 4.8b assures us that no grating lobes enter the visible region at the highest frequency. Thus, the logarithmic-rotated-subarray array seems to achieve the requirements for which it was designed. However, none of the previous figures give information about the near-in side lobes. For this reason, we have computed the radiation pattern with an average spacing of $0.1 \times 0.844\ \lambda$. As we have explained previously, we will obtain a close view of the main lobe. The result is shown in Figure 4.9.

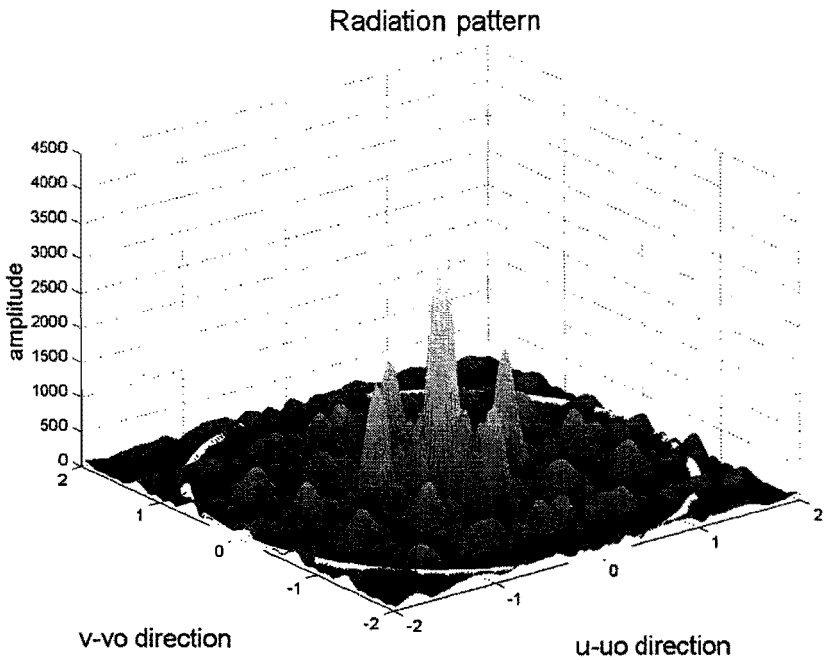

Figure 4.9. Radiation pattern of the logarithmic-rotated-subarray array for $\langle s \rangle = 0.1 \times 0.844\ \lambda$

Figure 4.9 shows high near-in side lobes; a cross section of this diagram gives a peak level for the side lobes of -10 dB. An interpretation based on the Fourier theory explains the presence of these high side lobes. In the conditions of Figure 4.9, the average spacing is $0.1 \times 0.844\ \lambda$, and the dimensions of the logarithmic-rotated-subarray array depicted in Figure 4.7 have to be divided by 10 (see § 4.1.2.b). Thus, the average spacing of each subarray becomes equal to $0.0667\ \lambda$ and it can be viewed as a full square aperture antenna. Figure 4.10 shows the new layout of the logarithmic-rotated-subarray array.

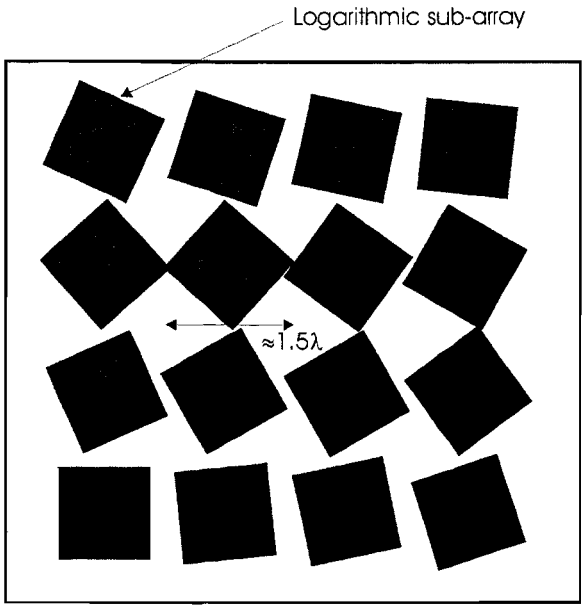

Figure 4.10. Layout of the logarithmic-rotated-subarray array with the original dimension divided by *10*.

As can be seen in Figure 4.10, there is a "periodic" blank lying between the subarrays with a "periodicity" of *1.5* λ in both directions. The blank area introduces in the Fourier domain an interfering signal localized at $u=\pm 1/1.5 \approx 0.6$ and $v \pm 1/1.5 \approx 0.6$. Figure 4.11 allows us to check out these locations.

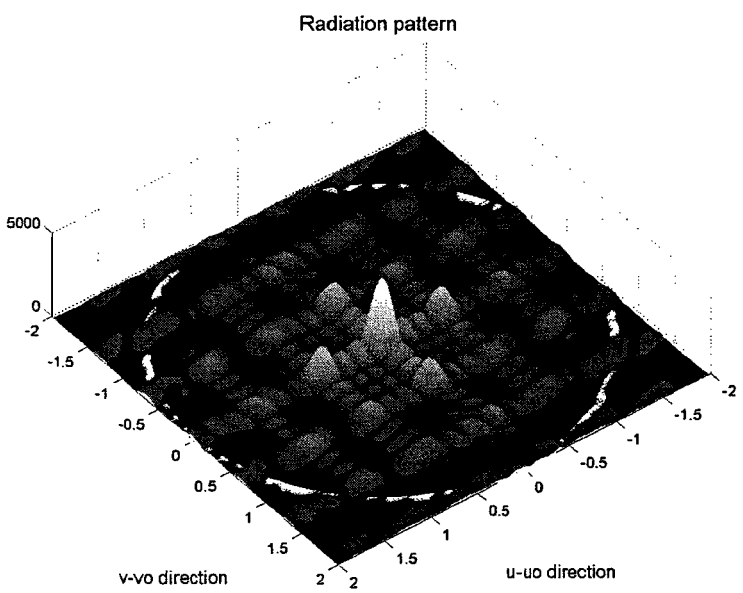

Figure 4.11. Locations of the blank perturbations.

4.2.3 Hexagonal-logarithmic-rotated-subarray array

In order to reduce the blank area between the rotated subarrays, we decided to take a hexagonal shape for these subarrays. The hexagon was chosen to fit in the square defined by the length of the logarithmic-rotated-subarray. Elements located within the hexagon are kept, the others are removed. Figure 4.12 shows an example of a hexagonal-logarithmic-rotated-subarray.

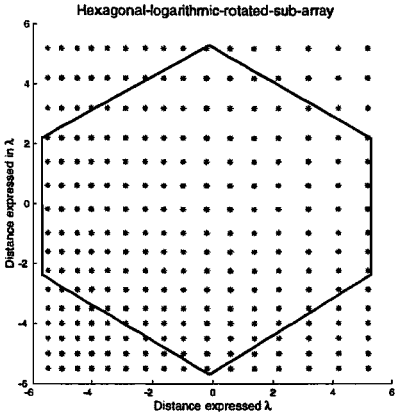

Figure 4.12. Example of a hexagonal-logarithmic-rotated-subarray.

The hexagonal shape of the subarrays results in a composite array with less elements than the previous one. Figure 4.13 shows the general layout of the array constructed by the rotation of *16* hexagonal-logarithmic-rotated-subarrays. It has *2565* elements with an average inter-element spacing *(s)* of roughly *0.468* λ. It may be surprising to obtain an average spacing smaller than $\lambda/2$. However, this average spacing is set for the lowest frequency. The radiation pattern of this array is given in Figure 4.14. It can be seen that the near-in side lobes have decreased considerably.

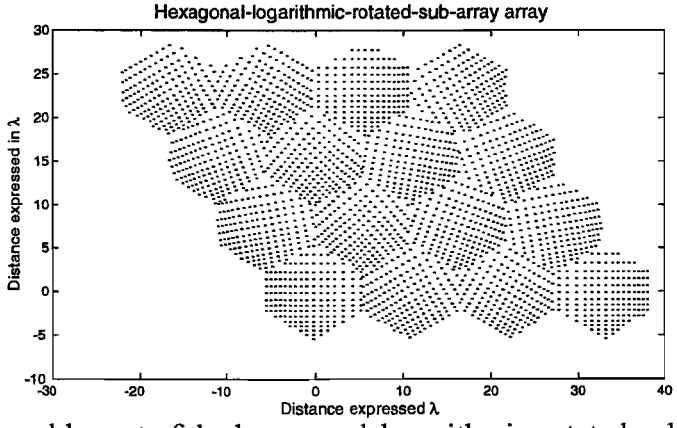

Figure 4.13. General layout of the hexagonal-logarithmic-rotated-subarray array. The total number of elements is *2565* with an average spacing of *0.468* λ

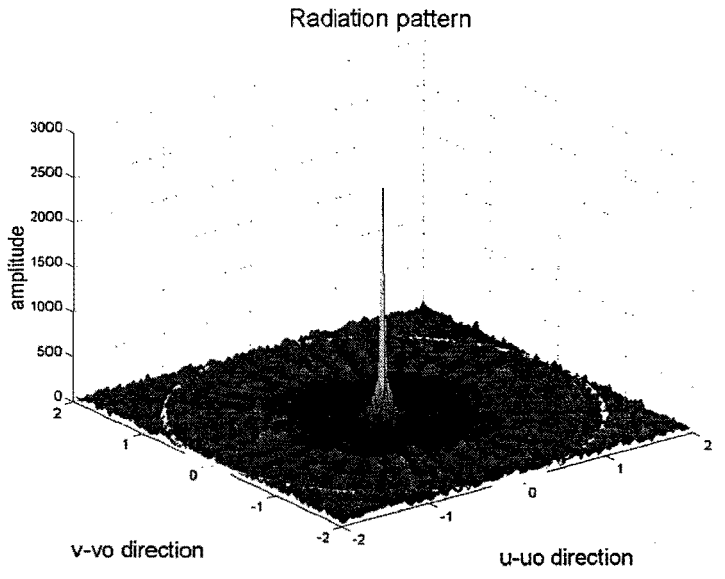

(a)

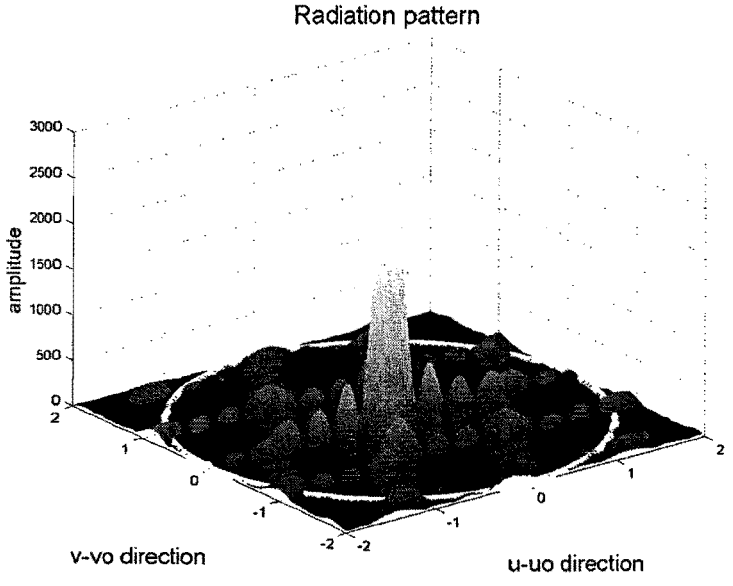

(b)

Figure 4.14. Radiation pattern of the hexagonal-rotated-logarithmic-subarray array. *(a) $\langle s \rangle = 1 \times 0.468\ \lambda$ (b) $\langle s \rangle = 0.1 \times 0.468\ \lambda$*

This array presents good characteristics. The level of the near-in side lobes has been reduced and no grating lobes have entered the visible region. However, the array configuration has the main drawback to present strong structural irregularities. There is no symmetry in the array, and the subarrays are not identical. This array would be difficult to build with patch antenna and mutual coupling would be unpredictable.

In summary, we have seen that the rotation of subarrays could lead to arrays presenting a broadband behaviour. But as soon as there is a "periodic" blank in the array configuration, the near-in side lobes increase dramatically. The filling of the blank areas reduced the near-in side lobes but will introduce strong mutual coupling.

4.3 Regular-perturbed array

Prof. Tijhuis suggested that we should investigate the field of regular arrays with small perturbations. In this section, we study the effect of random perturbations applied to the element locations. First, we present the perturbation model that we have applied to linear and planar regular arrays. Then, we evaluate the impact of such perturbations on the radiation pattern.

4.3.1 Perturbation model

Let us start with the case of a linear array of length, L, with N equally-spaced elements and with an inter-element spacing, d. We consider a random perturbation of the element locations. The element locations are affected in such a way that an array element will be slightly moved away from its original location. The random perturbation is modelled by a probability density function $p(\delta)$ described as follows,

$$p(\delta)\begin{cases} 1/q \; for -q/2 \le \delta \le q/2 \\ 0 \qquad otherwise \end{cases} \qquad (4.1)$$

where q is a relative distance and represents the degree of perturbation. It is expressed as a fraction of the inter-element spacing d, $-1 \le q \le 1$. For example, a perturbation of 0.4 means that the array element n originally placed at $x_n = nd$ will be positioned somewhere in the region bounded by $nd-0.4d$ and $nd+0.4d$. Figure 4.15 illustrates this example.

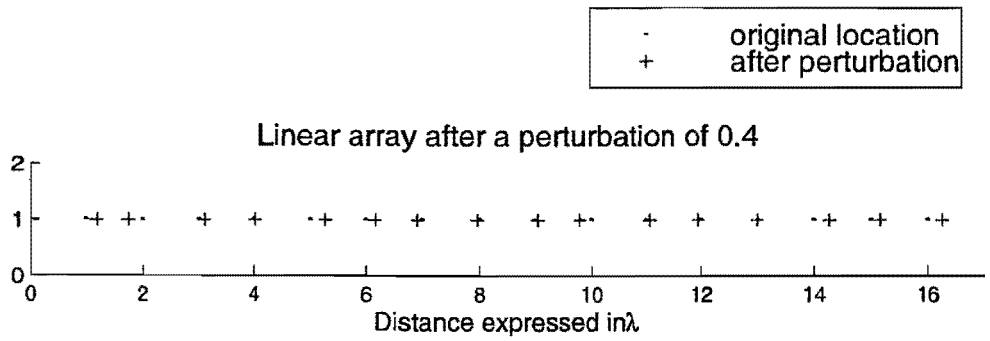

Figure 4.15. *16*-element linear array after a perturbation of *0.4*.

The normalized array factor of the array depicted in Figure 4.15 can be written as follows,

$$E(u) = \frac{1}{N}\sum_{n=1}^{N} a_n e^{jkux_n} \qquad (4.2)$$

where a_n is the amplitude of element n,

$$a_n = e^{jku\delta_n} \qquad (4.3)$$

δ_n is a distance and represents the perturbation on the element position. It follows the probability density function, $p(\delta)$, expressed in Equation (4.1). To obtain the average power pattern of the array, since δ is a statistical parameter, we have to evaluate the mathematical expectation of $E(u)$ multiplied by its complex conjugate

$$\left\langle |E(u)|^2 \right\rangle = \left\langle \frac{1}{N^2}\sum_{m=1}^{N}\sum_{n=1}^{N} e^{jku(\delta_m-\delta_n)} e^{jkud(m-n)} \right\rangle \qquad (4.4)$$

A convenient way to compute this expression is to perform the summation for $m=n$ and for $m\neq n$ separately.

$$\left\langle |E(u)|^2 \right\rangle_{m\neq n} = \frac{1}{N^2}\sum_{m=1}^{N}\sum_{n=1}^{N} \left\langle e^{jku(\delta_m-\delta_n)} \right\rangle e^{jkud(m-n)} \qquad (4.5)$$

The average of the term related to the random perturbation (for $m\neq n$) is

$$\left\langle e^{jku(\delta_m-\delta_n)}\right\rangle = \int\int e^{jku(\delta_m-\delta_n)} p(\delta_m)p(\delta_n)d\delta_m d\delta_n = \left(\frac{\sin(kuq/2)}{kuq/2}\right)^2 \tag{4.6}$$

After addition of the term corresponding to the case $m=n$ ($1/N$) to Equation (4.5), the expression for the power pattern becomes

$$\left\langle |E(u)|^2 \right\rangle = \left(\frac{\sin(kuq/2)}{(kuq/2)}\right)^2 |E_0(u)|^2 + \frac{\left(1-\left(\frac{\sin(kuq/2)}{(kuq/2)}\right)^2\right)}{N} \tag{4.7}$$

As we have seen in Chapter 3 the effect of a random perturbation is to produce an average power pattern that is the superposition of two terms. One term is the unperturbed power pattern multiplied by a factor depending on the location error. The other term depends on the location error only. In the next section, we draw some conclusions about the impact of random errors on the grating lobes level.

4.3.2 Effects on the grating lobes

The array depicted in Figure 4.15 has an inter-element spacing of one wavelength and grating lobes enter the visible region at $u=\pm 1$, as shown in Figure 4.16a. We evaluate in this section the impact of the random perturbation on the grating lobes. For simplicity, we define the random perturbation q with respect to the wavelength and we rewrite Equation (4.7) as follows,

$$\left\langle |E(u)|^2 \right\rangle = A|E_0(u)|^2 + (1-A)\frac{1}{N} \tag{4.8}$$

$$\text{where } A = \left(\frac{\sin(X)}{X}\right)^2, X = 2\pi u \frac{q}{\lambda}$$

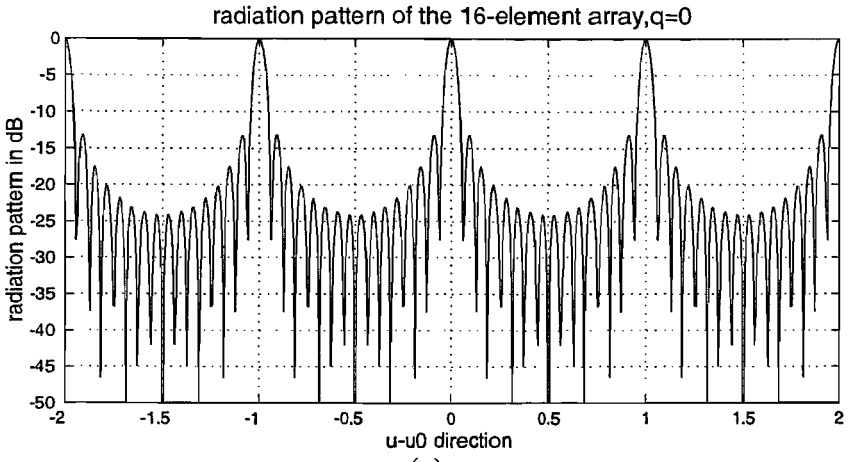

(a)

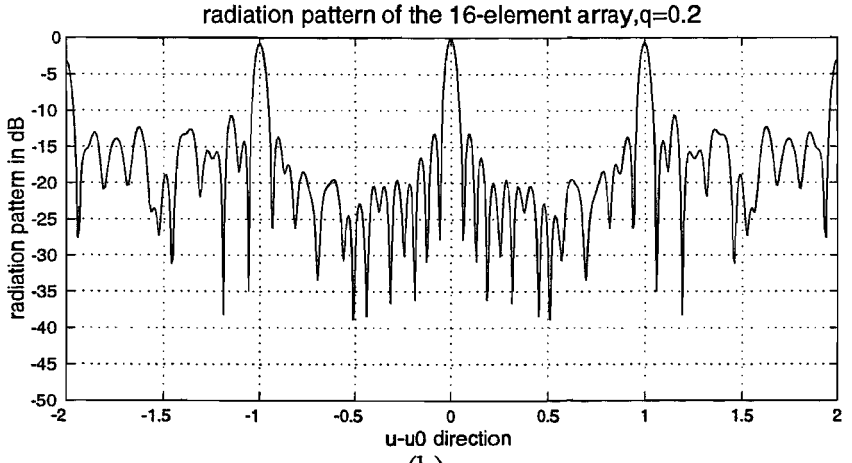

(b)

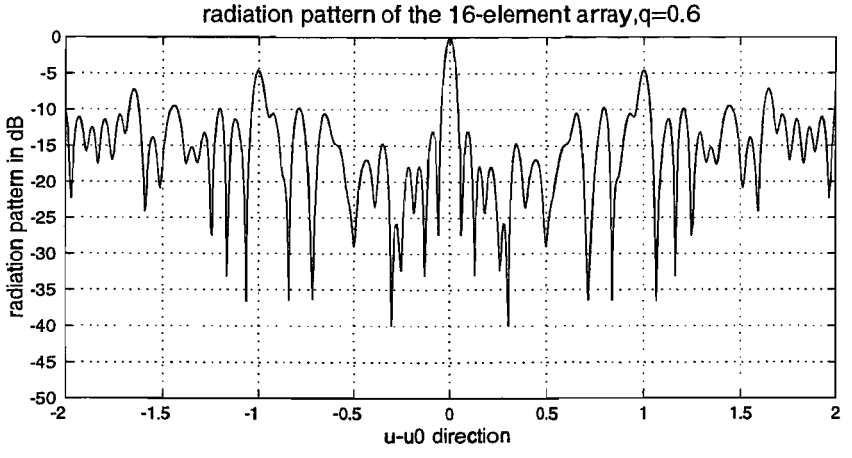

(c)

Figure 4.16. Radiation pattern of a *16*-elements linear array, with an inter-element spacing $d = \lambda$. (a) $q=0$. (b) $q=0.2$. (c) $q=0.6$.

As soon as we apply a perturbation on the element locations, the lobes located at $u = \pm 1$ cannot be called 'grating lobes' anymore, because their amplitudes become smaller than the main lobe. For convenience sake, we will call them grating lobes.

Figure 4.16b shows that a small perturbation of *0.2*, does not affect the grating lobes. For a perturbation of *0.6* the level of these grating lobes decreases only by *5* dB . Equation 4.8 shows that the unperturbed power pattern $|E_0(u)|^2$ is weighted by a factor proportional to the location error, called the error coefficient. To evaluate the impact of this error coefficient on the initial power pattern, we have plotted this coefficient for various values of q in Figure 4.17.

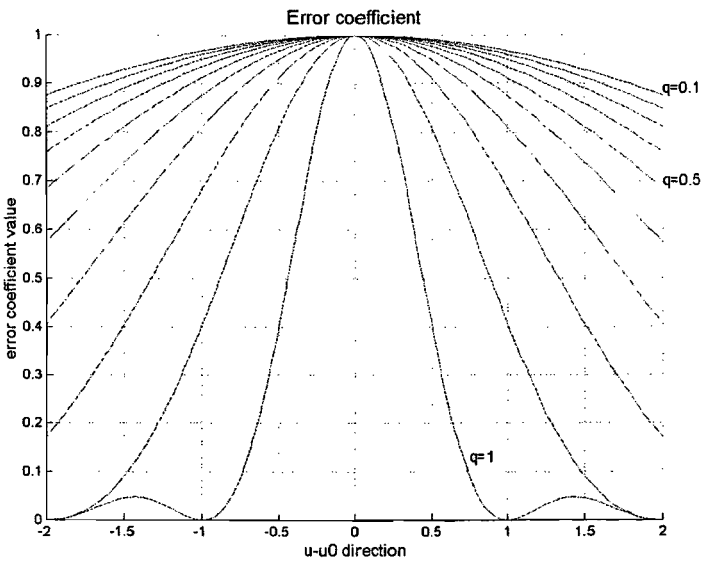

Figure 4.17. Error coefficient for different degrees of perturbation q.

The error coefficient affects the levels of the grating lobes slightly. If we apply a substantial perturbation of *0.5,* the grating-lobe level is reduced by only *10 %.* A perturbation of *0.9,* which generates an almost random array results in a grating-lobe level of *40 %* of its initial value. Of course, a perturbation of *1* suppresses the grating lobes completely. Actually, for a perturbation of *1*, the grating lobes become side lobes with a level expected at *10log(N)*, where N is the number of elements, as in a random array.

In order to complete this remark we have plotted in Figure 4.18 the grating-lobe level versus the degree of perturbation.

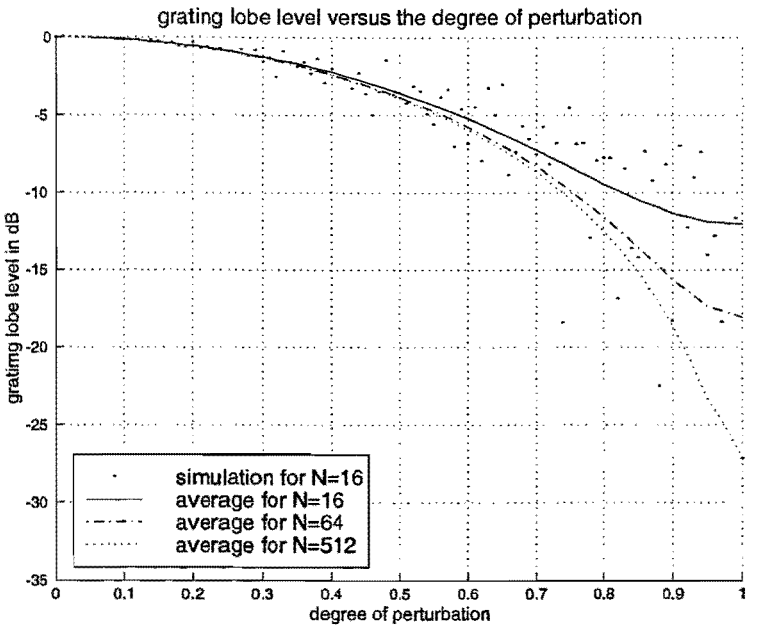

Figure 4.18. The grating lobe level versus the degree of perturbation.

In Figure 4.18, the solid line represents the average of the grating lobe levels for a *16*-element linear array and the dots stand for the grating-lobe level obtained by simulation. We have also plotted the average of the grating lobe levels of a *64*-element array (dash-dotted line) and a *512*-element array (dotted line). Irrespective of the number of elements of the array, it is shown that up to a perturbation of *0.6* the grating lobe levels decrease on average by only *–5* dB. Near a perturbation of *1*, the average of the grating lobe level approaches the value predicted by the theory: *–12* dB for a *16*-element array, *-18* dB for a *64*-element array and *–27* dB for a *512*-element array.

In summary, spatial random perturbations have a weak effect on the level of the grating lobes of a regular array. Up to a perturbation of *0.6*, which means that an element is located somewhere in an interval centered on its original location and with a width of *0.6* time the wavelength, the grating-lobes level decreases only by *5* dB. Thus regular arrays present strong robustness against random perturbation.

4.4 Radial-density-tapered array

In Chapter 2, it has been established that an array can be considered as a sampled aperture; array elements sample the current density function *I(x)* of a conventional aperture used as a model. The theory has shown that if we approximate an aperture with a regular sampling function with a sampling step of $\lambda/2$, no grating lobes enter the visible region, but this requirement has revealed to be unrealizable for the design of SKA.

In this section, an aperiodic sampling function is presented. This function is based on a new radial density taper method. In the first part, we present the principle of density taper in one dimension and then, we extend this principle to a planar array. Finally, we end up with a new radial density taper.

4.4.1 Presentation

We consider here a continuous linear antenna of length *L*. We call *N* the number of elements obtained after the sampling of the antenna. To employ density tapering, an amplitude taper illumination function *I(x)* is selected as a model. One criterion for its selection is that, when used with a continuous aperture, its radiation pattern should be similar to that desired of the density tapered array. The illumination function of the amplitude tapered model that we have chosen is depicted in Figure 4.19a. To locate the positions of the *N* elements the area under the curve is divided into *N* equal parts and an element is placed at the centre of each of the intervals defined by equal areas, as illustrated in Figure 4.19b. The density of the equally excited, unequally spaced, discrete currents depicted in (b) is seen to approximate the continuous current density function of (a).

The justification for considering the density taper method of unequally spaced array design is that the discrete, equally excited currents of the array elements approximate the continuous-aperture amplitude-taper illumination function used as a model. But there is no guarantee that the radiation pattern of the density tapered array will be suitable approximation to the radiation pattern of the amplitude tapered model. For more details, we refer the reader to the work of Doyle [18].

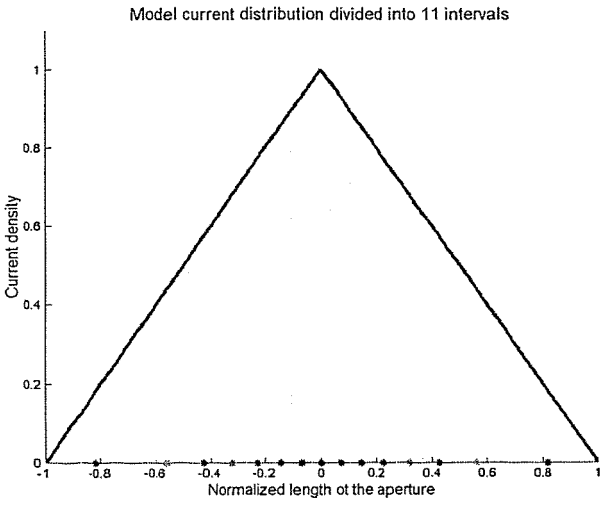

Figure 4.19a. Model current-density illumination function divided into *10* intervals.

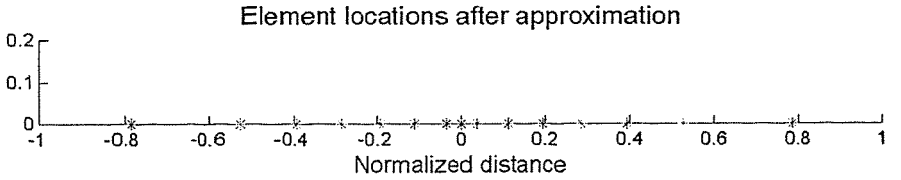

Figure 4.19b. Location of density tapered elements

To illustrate the density taper method, we consider a linear array with a length of *20* λ If we sample this antenna with a uniform sampling function, we will end up with *40* elements. By applying the density taper method presented previously, the number of elements drops to *15*, which is *30 %* of the number required for a filled periodic array. Moreover, the first side lobe of the continuous, an aperture with a triangular taper is *26* dB below the main lobe. Figure 4.20 shows the radiation pattern for the *15*-element, aperiodic array displayed above.

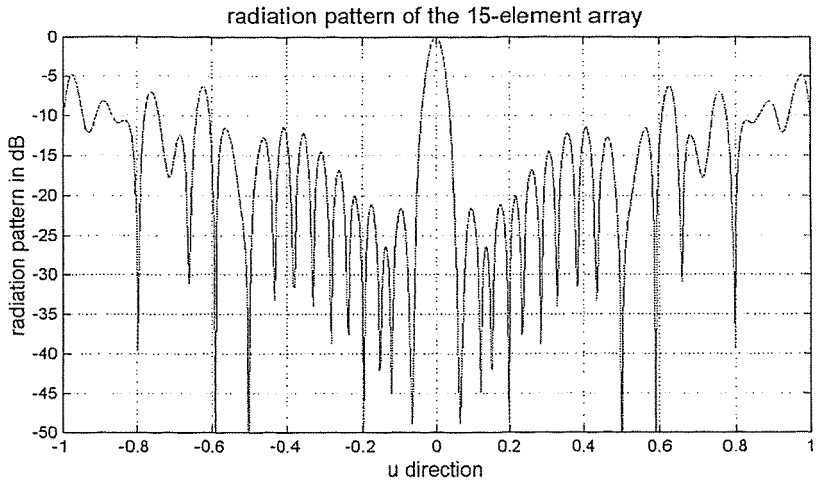

Figure 4.20. Radiation pattern of the *15*-element aperiodic array.

Figure 4.20 presents a cutting out of the radiation pattern similar to the one of the radiation pattern of the logarithmic *row*-array (see Section 4.2.1.a). Once again, the radiation pattern may be broken into *3* regions. The first region is located around the main lobe and includes the near-in side lobes. Here the radiation pattern exhibits an approximation to the design properties; the side lobes are controlled. The level of the first three side lobes is around *–25* dB which is close to the expected value of *–26* dB for a triangular amplitude taper [15]. The next region is a transition region, in which the side lobe pattern degenerates from the design characteristics toward that of the random array. In the third region, the average side lobe level is close to that of a random array.

For a planar array it is not obvious to find a technique that well approximates the amplitude taper, illumination function. Statistical thinning procedures appeared to be unsuitable for the design of SKA and a procedure based on the approximation of the integral aperture illumination is tedious to use. This problem has brought us to develop a technique based on the work of Anderson [19] that accurately approximates a two-dimensional illumination function.

4.4.2 A new density taper method

4.4.2.a The geometrical transformation

We have seen in Section 3.1.2 that a thinning procedure removes elements from a regular grid according to an amplitude taper illumination function used as a probability density function. We have concluded that it enables a reduction of the number of elements and the control of side lobes, but it does not suppress grating

lobes. From these observations, we have developed a technique that eliminates the underlying grid by keeping the same density of elements found for the thinned array.

Let us consider a uniform circular array with the elements positioned on a regular grid with a triangular lattice as depicted in Figure 4.21. An element p of the array is defined by its polar coordinates (r_p, φ_p), where r_p is its normalized radius ($1 \leq r_p \leq 0$).

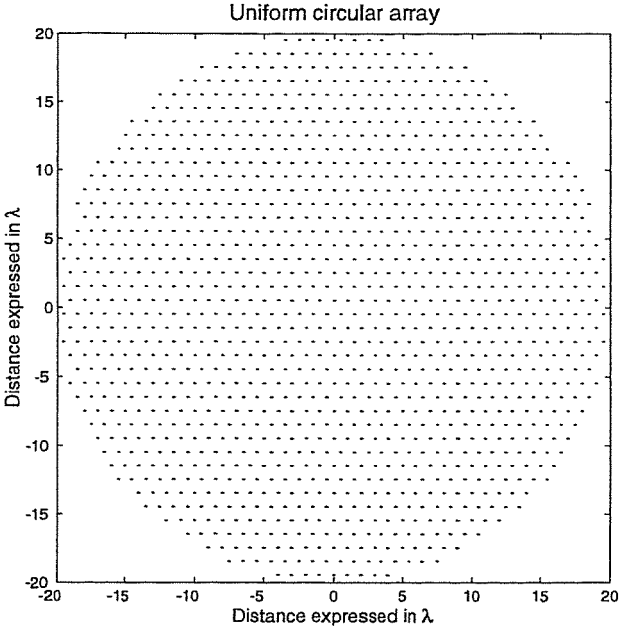

Figure 4.21. Uniform circular array of *1258* elements and an inter-element spacing equal to λ

We call D the radial density of the uniform array and D_t the radial density of the thinned array. Since D is the radial density of the array, the number N of elements in a ring of normalized radius, r, and width, dr, is approximately,

$$N = 2\pi r dr D.$$

In Section 3.1.2 of Chapter 3, we have thinned an array statistically by using an amplitude taper reference $A(r)=a+(1-a)\cos^2(\pi r/2)$, where a is a constant. It can be shown that the radial density of the thinned array is,

$$D_t(r)=A(r)D \quad (4.9)$$

The principle of this new procedure is to find a geometrical transformation, $h(r)$, that maps the elements of the array, defined by (r, φ) to new locations, defined by $(h(r), \varphi)$, in such a way that the radial density of the resulting array will equal the radial density of the thinned array D_t.

Furthermore, we should have $h(0)=0$ so that there is no change in the position of the element at the centre of the aperture and $h(1)=1$ so that the edge of the array does not change.

In the uniform array, the number of elements in a ring defined by radius r and width dr is,

$$N = 2\pi r dr D \quad (4.10)$$

After the geometrical transformation, these elements are mapped onto a ring of radius $h(r)$ and width dh. Hence,

$$N = 2\pi h(r) dh(r) D_t\{h(r)\} \quad (4.11)$$

Substitution of Equations (4.9) and (4.10) into (4.11), leads to a differential equation for h,

$$\frac{dh(r)}{dr} = \frac{r}{A[h(r)]h(r)}, \text{ for } r \in [0,1] \quad (4.12)$$

Since $A(r)$ is a pedestal, cosine-squared function ($A(r)=a+(1-a)\cos^2(\pi r/2)$, where a is a *constant*), no analytical solution is available to solve Equation (4.12). We numerically compute Equation (4.12), by applying a discretization of the spatial coordinate as follows,

$$\begin{aligned} r_n &= n\Delta r \\ h(r_n) &= h(n\Delta r) = h(n) \\ \frac{dh(r_n)}{dr} &= \frac{h((n+1)\Delta r) - h(n\Delta r)}{\Delta r} = \frac{h(n+1) - h(n)}{\Delta r} \end{aligned} \quad (4.13)$$

Equation (4.12) leads to the following discrete equation

$$h(n) = \frac{(n-1)\Delta r}{A[h(n-1)]h(n-1)}\Delta r + h(n-1) \quad (4.14)$$

We have taken $\Delta r = 0.0005$, and ensured $h(r=1)=1$ by adjusting the slope of the curve at the origin. We have computed h for two types of amplitude taper references:

a pedestal, cosine-squared, function and a parabola. Figure 4.22a shows the amplitude taper functions and Figure 4.22b presents the geometrical transformation, *h(r)*, corresponding to the two types of illumination functions.

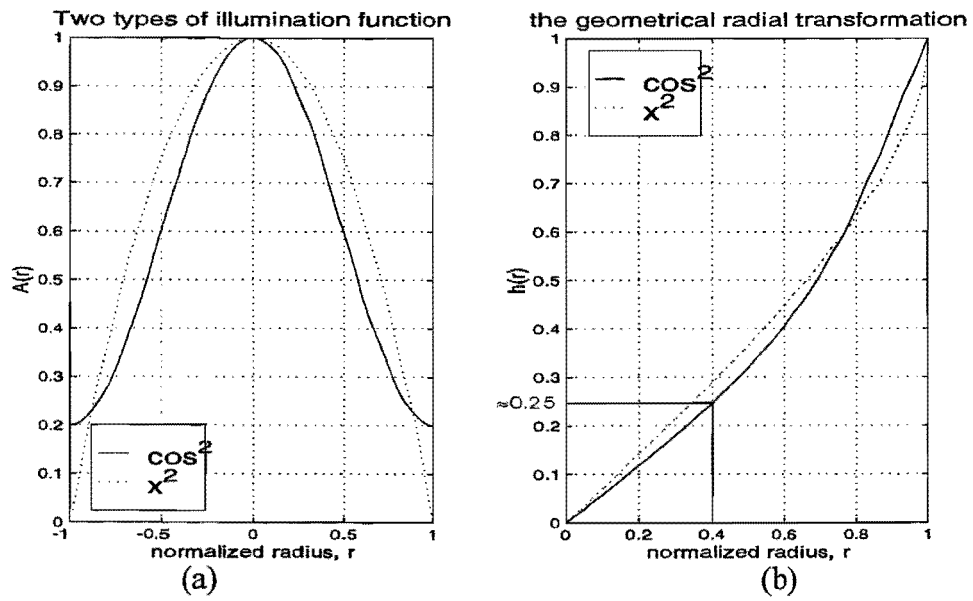

Figure 4.22. (a) Example of two types of illumination functions a pedestal cosine-squared function and a parabola. (b) Corresponding geometrical transformation, *h(r)*.

4.4.2.b Results

Figure 4.21 presents the layout of a uniform circular array of *1258* elements placed on a regular triangular lattice. The inter-element spacing is λ, and grating lobes enter the visible region, as shown in Figure 4.23. Because of the triangular lattice, these grating lobes occur on a circle of radius of *1* (λ / *spacing*) in the *uv*-plane, at angles of $p\pi/6$ ($p = 0, 1, 2, 3, 4, 5$) [20].

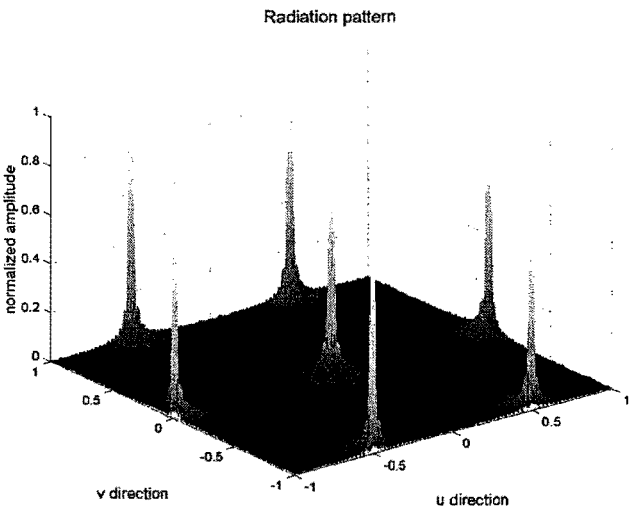

Figure 4.23. Radiation pattern of the uniform circular array *1258* elements and an inter-element spacing equal to λ.

The geometrical transformation, *h(r)*, corresponding to a pedestal, cosine-squared, function has been applied to the uniform array shown in Figure 4.21. The results are depicted in Figure 4.24.

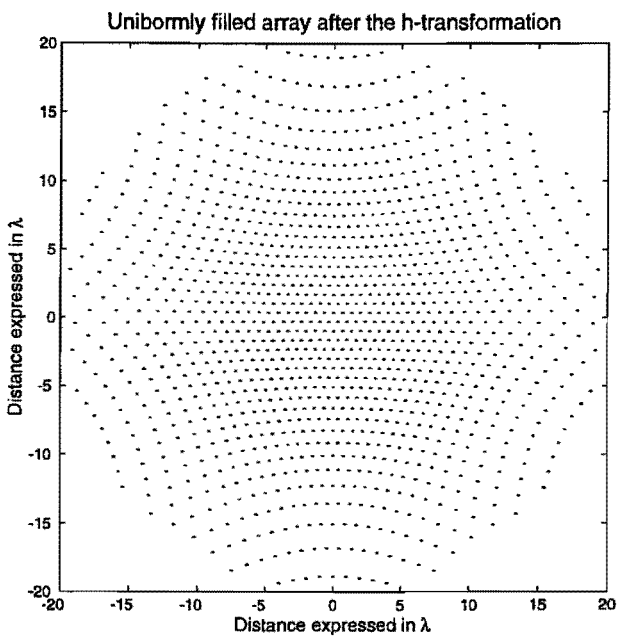

(a)

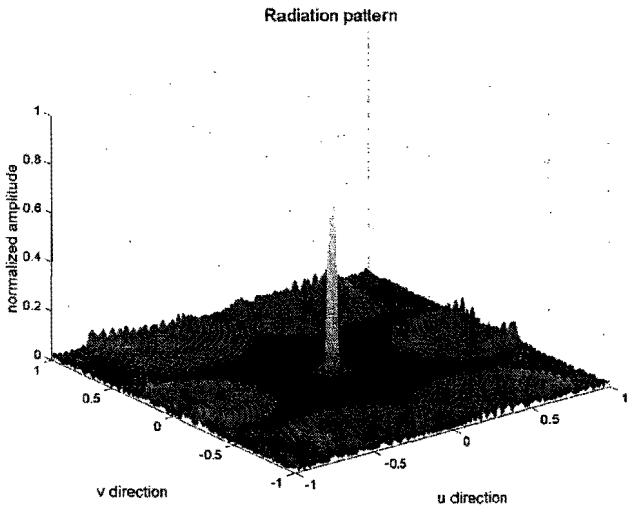

(b)

Figure 4.24. (a) Uniform array after the *h*-transformation; *1258* elements; average spacing, $\langle s \rangle = \lambda$ (b) Corresponding radiation pattern.

In Figure 4.22b, it is shown that for $0 \leq r \leq 0.8$, the gradient of function h is smaller than *1*, and for $0.8 \leq r \leq 1$, the gradient is larger than *1*. So, elements near the centre of the array are squeezed together while the elements near the edges are stretched, as shown in Figure 4.24a. In the original grid the elements were positioned in rows; because the radius for each element in a row is different, the row is bent after the *h*-transformation.

The transformation of the original, underlying grid leads to the suppression of the grating lobes, as shown in Figure 4.24b. It results in an array, with an element density approaching the illumination function. The choice of the amplitude taper function used for the computation of *h*, offers the possibility to control the near-in side lobes, as shown in Figure 4.25.

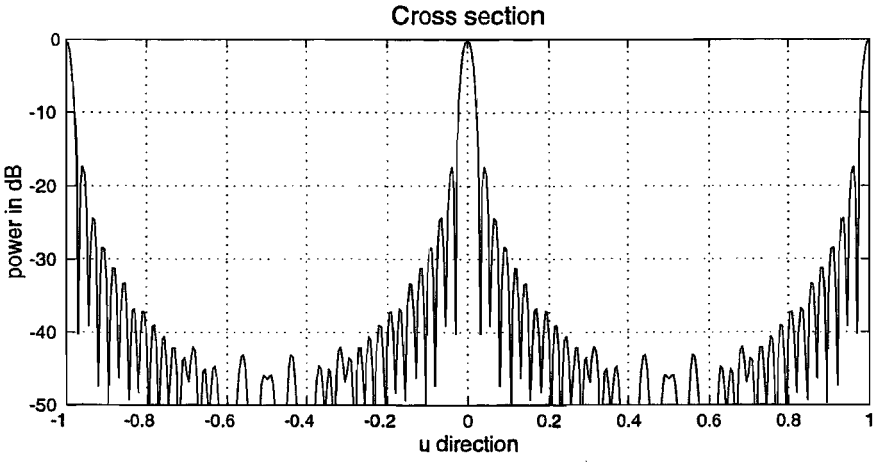

(a)

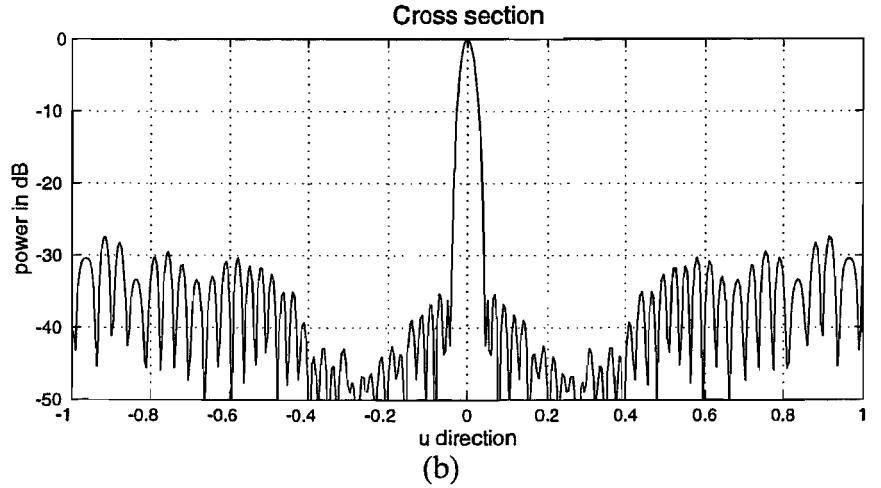

(b)

Figure 4.25. Cross section of the radiation pattern at $v = 0.$ (a) Uniform array. (b) After the transformation.

The near-in side-lobe level of the uniform array is about -17dB, as shown in Figure 4.25a, which corresponds to the expected value for a circular aperture [20]. Figure 4.25a also shows the expected grating lobes positioned at *(-1,0)* and *(1,0)*. Figure 4.25b exhibits a near-in side-lobe level of roughly -35 dB, which should be compared with the value expected for a continuous aperture tapered with a pedestal cosine-squared.

For $r \leq 0.4$, Figure 4.22b shows that $h(r)$ is almost linear, with a gradient of 0.625. Thus, in the original array, the elements, lying within a circle of radius $r = 0.4$,

are transformed into a uniform circular array of radius, $h(r) \approx 0.25$, with a triangular lattice of 0.625 . This will cause, in the radiation pattern, six high side lobes. They are located on a circle of radius $r \approx 1.6$ (/ 0.625). By increasing the frequency, these high side lobes enter the visible region. Figure 4.26 shows the radiation pattern of the transformed array, computed for an average spacing of 2 .

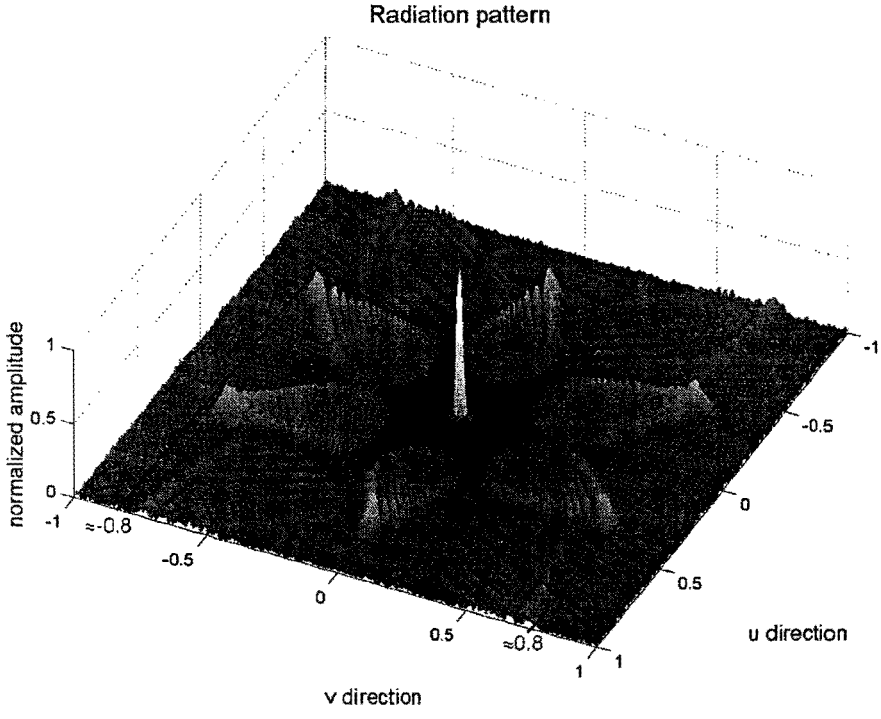

Figure 4.26. Radiation pattern of the uniform array after the h-transformation, 1258 elements, average spacing $\langle s \rangle = 2$.

In Figure 4.26, the frequency has been doubled, so the radius of the circle where the side lobes are positioned is ≈ 0.8. The six high side lobes are shown.

In order to suppress the periodicity introduced by the regular, underlying grid of the uniform array with a triangular lattice, we apply the radial transformation to a circular ring array. The original, circular, ring array consists of 20 concentric rings. The spacing between two consecutive rings equals the inter-element spacing within a ring. This spacing has been set to . The array has 1321 elements. Figure 4.27a shows the layout of the original circular ring array. After transformation, the rings with an original normalized radius smaller than 0.8 are squeezed together, while the others are stretched, as shown in Figure 4.27b. Figures 4.28 and 4.29 show the corresponding radiation patterns computed with $\langle s \rangle =$.

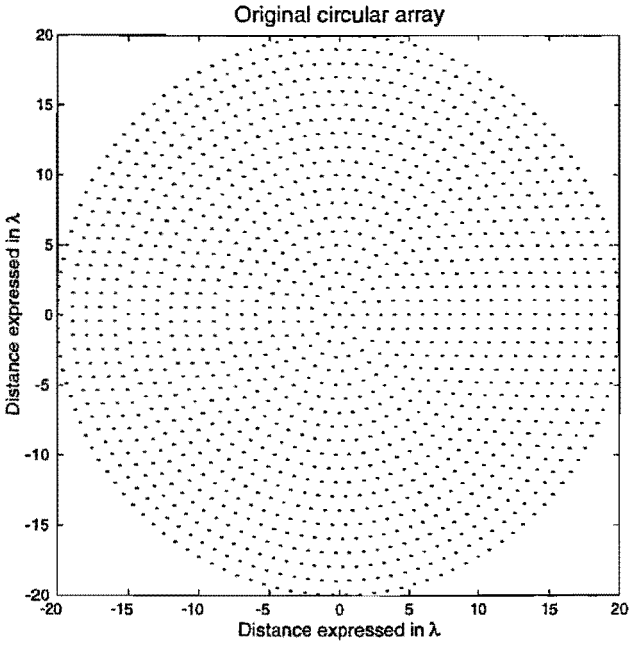

(a)

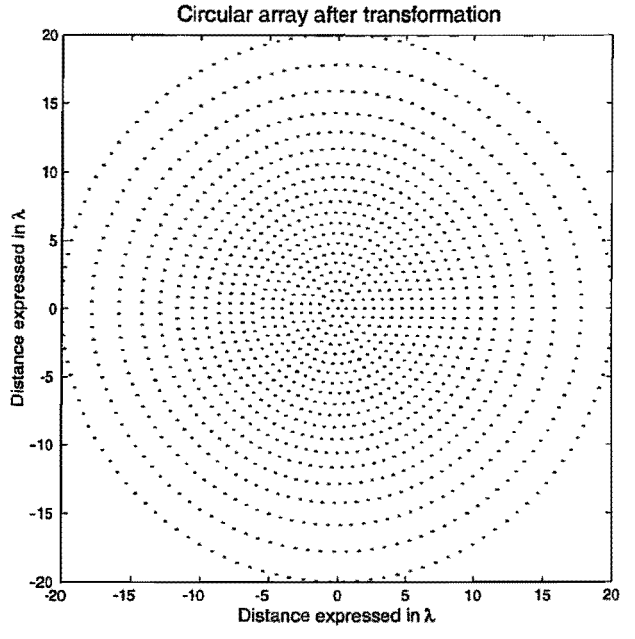

(b)

Figure 4.27. General layouts. (a) Original, circular, ring, array; *1321* elements; average spacing $\langle s \rangle = \lambda$ (b) Circular ring array after the *h*-transformation.

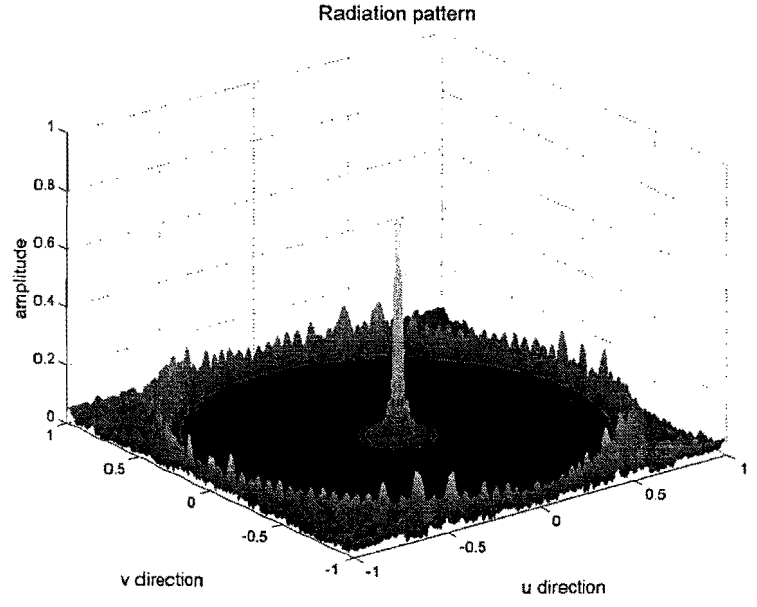

(a)

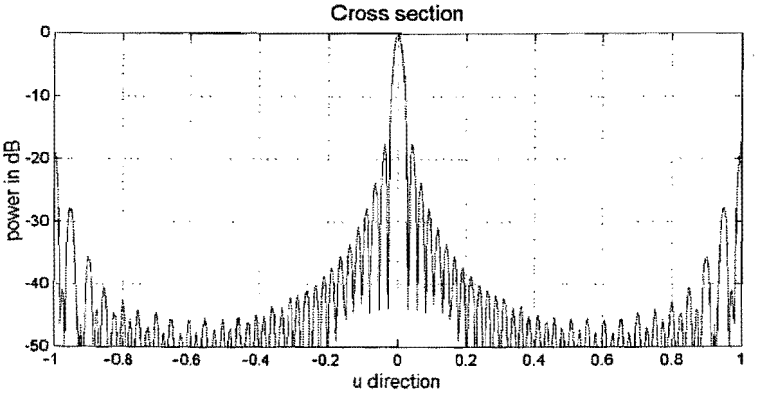

(b)

Figure 4.28. (a) Radiation pattern of the original circular ring array, with *1321* elements, $\langle s \rangle = \lambda$ (b) Cross-section at $v=0$.

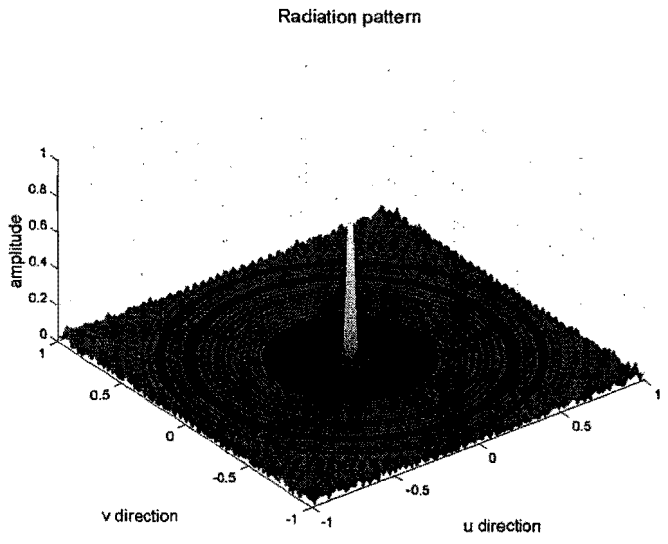

(a)

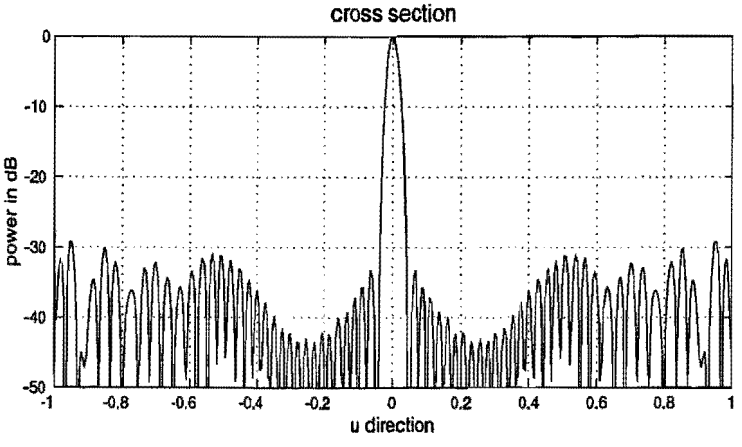

(b)

Figure 4.29. (a) Radiation pattern of the circular ring array after transformation, with *1321* elements, $\langle s \rangle = \lambda$ (b) Cross-section at $v=0$.

The radiation pattern of the original circular ring array, shown in Figure 4.28a, exhibits high side lobes lying along a circle. These side lobes are due to the radial periodicity of the original array. Indeed, the rings of the original array are equally spaced with an inter-ring spacing of λ. This radial periodicity leads to a circle frequency of radius equal to *1* (λ/*spatial periodicity*) in the *uv*-domain. A cross-section of Figure 4.28a, shown in Figure 4.28b, gives the side-lobe level induced by this spatial periodicity.

Applying the geometrical transformation, *h(r),* to the original circular ring array results in the suppression of this radial periodicity. Figure 4.29a and Figure 4.29b show that no perturbing frequency appears in the radiation pattern. It is shown that side lobes are controlled over the visible region. However, at higher frequencies, the side lobes are not controlled anymore, and their properties tend toward those of a random array. Figure 4.30 shows a cross-section of the radiation pattern for $\langle s \rangle = 2\lambda$.

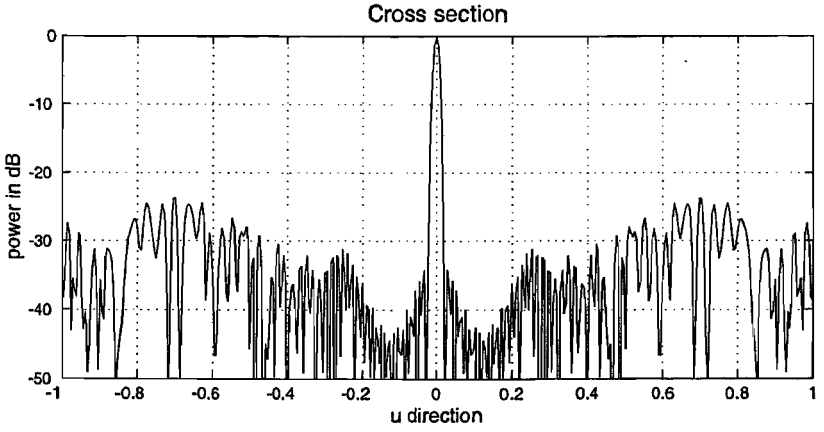

Figure 4.30. Cross-section of the radiation pattern of the transformed circular array, $N=1321$, $\langle s \rangle = 2\lambda$.

For $|u| \leq 0.3$, the side lobes are controlled, this region corresponds to the one shown in Figure 4.29b. For $|u| \geq 0.3$, the side-lobe level fluctuates around -30 dB ($-10\log(1321) \approx -31$), as expected for a random array.

As it has been explained previously, the transformed array still presents a radial periodicity for $h(r) \leq 0.25$, which introduces perturbations in the *uv*-domain. It explains the peak, side-lobe level at $u \approx 0.8$ in Figure 4.30.

In summary, since the radial, geometrical transformation presents an almost linear behaviour for small values of *r*, the structure of the original array is important. An array with a periodic structure introduces perturbations in the *uv*-domain. In the case of a circular array with a regular underlying grid, high side lobes appear, whereas a ring array limits this drawback.

The near-in side lobes, in both cases are controlled. It means, that the function h is a good approximation of the illumination function.

4.5 Conclusion

The logarithmic spacings in subarrays result in a broadband behaviour, and rotations smear the high side lobes in the *uv*-domain. However, a periodic blank between subarrays introduces high near-in side lobes. Filling this blank can reduce them. A way to do that is to take subarrays with a hexagonal shape, and place them side by side. However, the resulting structure is complex and leads to strong coupling and construction difficulties.

An easy alternative procedure would have been to place elements on a regular grid, spaced at some wavelength apart, and slightly perturb the element locations. We have expected that the grating lobes might disappear. It turned out, that random perturbations do not really affect the grating-lobe level.

The radial density taper method presents the advantages of suppressing the grating lobes, and of controlling the near-in side lobes. Implicitly, the principle of rotations was exploited by considering a circular array. The regularity of the resulting configuration may facilitate the mutual coupling analysis. Finally, this pre-defined density function can be obtained in a systematic way.

Chapter 5

Conclusions and Recommendations

In this report, we have studied different types of configurations for the Square Kilometer Array. The main difficulty was to find configurations presenting a broadband behaviour, without grating lobes and a reasonable number of elements, over a frequency decade. We tried to find a systematic approach for the analysis of the configurations to be compared. The configuration should not only have a low side-lobe level but also a locally regular structure. It means that the array spacing should change gradually. For the latter reason, we avoided statistical thinning and random arrays. These configurations are not regular, and each antenna in the array presents a different electromagnetic environment. Thus, each array element would require a different design to achieve impedance matching.

An exhaustive literature review on aperiodic arrays revealed three types of design procedures. All of these share the features of suppressed grating lobes and a low side-lobe level. However, they differ in their construction, and they do not offer the same simplicity for a mutual coupling analysis.

A first approach has lead to a logarithmic array. This array is locally regular and exhibits a gradual logarithmic change in its inter-element spacing, which allows antenna matching. However, a cross of high side lobes in the *uv*-domain, limits its usefulness. Designing an array with rotated subarrays similar to the original logarithmic array reduced this cross. However, the resulting structure presented blank areas between the subarrays, which lead to high near-in side lobes. A hexagonal shape for the subarrays allowed a closely-packed arrangement, which reduced the side-lobe level, but the construction would be difficult.

A regular array with equally spaced elements would have been an attractive configuration for its easiness of construction and to accurately model the mutual coupling. We thought that small perturbations applied to the element locations might suppress the grating lobes due to an inter-element spacing larger than the allowable distance. However, a study revealed that grating lobes are only slightly affected by the perturbations, as long as they are much smaller than the wavelength.

Finally, a radial density taper method applied to a ring array structure gave good results. Firstly the use of a circular structure allowed a homogenous azimuthal distribution of the distant side lobe energy. Then, a radial density taper of the array enabled us to control the shape of the main lobe and the near-in side-lobe levels. The general layout presents some regular features, useful for its construction and the mutual coupling analysis. It is important to note that the radial transformation used in this approach can be determined, in a systematic manner, by the choice of the reference amplitude illumination function.

Further research may be carried out to ensure an element density that is equal in radial and azimuthal directions. This research should also evaluate how this structure may be constructed by using Vivaldi antennas.

Bibliography

[1] A. van Ardenne and F. M. A. Smits, "Technical aspects for the Square Kilometer Array Iterferometer", *ESTEC Workshop on Large Antennas in Radio Astronomy, The Netherlands,* pp 117–127, WPP–110, February, 1996.

[2] R. Braun, "The Square Kilometer Array Iterferometer", *The Westerbork Observatory, Continuing Adventure in Radio Astronomy,* pp 167–184. Edited by E. Raimond and R. O. Genee, Kluwer, Dordrecht.

[3] H. Unz, "Linear arrays with arbitrarily distributed elements", *IRE Transactions on Antennas and Propagation,* Vol. AP-8, pp 222–223, March, 1960.

[4] D. D. King, R. F. Packard, and R. K. Thomas, "Unequally spaced broadband antenna arrays", *IRE Transactions on Antennas and Propagation,* Vol. AP-8, pp 380–385, July, 1960.

[5] G. W. Swenson, and Y. T. Lo, "The University of Illinois Radio Telescope", *IRE Transactions on Antennas and Propagation,* Vol. AP-9, pp 9–16, January, 1961.

[6] R. E. Willey, "Space tapering of linear and planar arrays", *IRE Transactions on Antennas and Propagation,* Vol. AP-10, pp 369–377, July, 1962.

[7] M. I. Skolnik, J. W. Shermon, and F. C. Ogg, "Statistically designed density-tapered arrays", *IEEE Transactions on Antennas and Propagation,* Vol. AP-12, pp 408–417, July, 1964.

[8] R. J. Mailloux, and E. Cohen, "Statistically thinned arrays with quantized element weights", *IEEE Transactions on Antennas and Propagation,* Vol. AP-39, pp 436–447, April, 1991.

[9] A. L. Maffet, "Array factors with nonuiform spacing parameter", *IRE Transactions on Antennas and Propagation,* Vol. AP-10, pp 131–136, March, 1962.

[10] B. Holst, and W. Dennis, "Antenna array for grating lobe and sidelobe suppression". Patent, *serial number* 299660.

[11] I. Kaploun, "Sparse arrays", PATO course TU Delft, 1997.

[12] V. D. Agrawal, "Grating-lobe suppression in phased arrays by subarray rotation", in *Proceeding of the IEEE*, Vol. 66, NO. 3, March, 1978.

[13] Y. T. Lo, "A mathematical theory of antenna arrays with randmoly spaced elements", *IRE Transactions on Antennas and Propagation*, Vol. AP-12, pp 257–268, May, 1964.

[14] A. R. Panicali, and Y. T. Lo, "A probabilistic approach to large circular and spherical arrays", *IEEE Transactions on Antennas and Propagation*, Vol. AP-17, pp 514–522, July, 1969.

[15] B. D. Steinberg, *Principles of Aperture and Array System Design.* New York: Wiley, 1976.

[16] R. L. Fante, G. A. Robertshaw, and S. Zamoscianyk, "Observation and explanation of an unusual feature of random arrays with a nearest-neighbor constraint", *IEEE Transactions on Antennas and Propagation*, Vol. AP-39, pp 1047–1049, July, 1991.

[17] C. Craeye, "Broadband array for SKA", *Internal report*, ASTRON, 1999.

[18] W. Doyle, "On approximating linear array factors", *RAND Copr. Mem. RM-3530-PR,* February, 1963.

[19] P. D. Anderson, M. A. Ingram, and V. K. Tripp, "A new density tapering method based on radial warping", *IEEE Transactions on Antennas and Propagation*, Vol. AP-46, pp 1763–1764, November, 1998.

[20] R. E .Collin and F. J. Zucker, *Antenna Theory,* McGraw-Hill, 1969.